COLLEGE OF NATURAL AND COMPUTATIONAL SCIENCES

SCHOOL OF EARTH SCIENCES

APPLICATIONS OF GEOPHYSICAL TECHNIQUES IN THE INVESTIGATION OF GROUNDWATER CONTAMINATION FROM TANNERIES AND SLAUGHTER HOUSES NEAR MOJO RIVER, MAIN ETHIOPIAN RIFT, ETHIOPIA

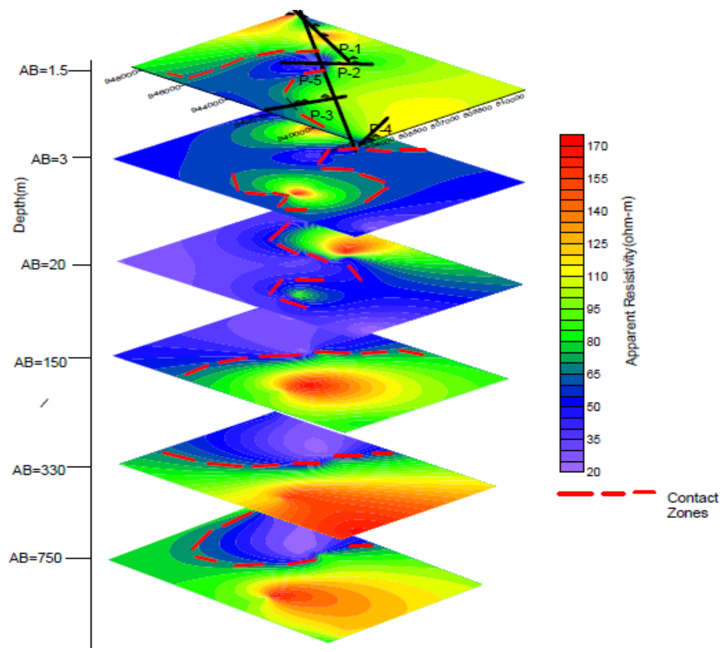

A Thesis Submitted to the School of Earth Sciences of Addis Ababa University in Partial Fulfillment of the Requirements for the Degree of Master of Science in Exploration Geophysics

By

Bekelu Abeba Mamo

June 2020

Addis Ababa

Approval page

This MSc. Thesis proposal entitled **"APPLICATION OF GEOPHYSICAL TECHNIQUES IN THE INVESTIGATION OF GROUNDWATER CONTAMINATION FROM TANNERIES AND SLAUGHTERHOUSES NEAR MOJO RIVER, MAIN ETHIOPIAN RIFT, ETHIOPIA** "approved in partial fulfillment of the requirement for the degree of Master of Science in **Exploration Geophysics**.

Submitted by:

Bekelu Abeba	_______________	____________________
Student Name	**Signature**	**Date**

Recommended By:

Prof. Tigistu Haile	_______________	____________________
Advisor	**Signature**	**Date**
Dr. Dessie Nedaw	_______________	____________________
Co-Advisor	**Signature**	**Date**
Dr. Abera Alemu	_______________	____________________
Examiner	**Signature**	**Date**
Dr. Shimeles Fisseha	_______________	____________________
Examiner	**Signature**	**Date**

Endorsed by:

__________________	_______________	____________________
School of Earth Science	**Signature**	**Date**
__________________	_______________	____________________
Associate Director, Post Graduate program	**Signature**	**Date**

ABSTRACT

A study aimed is identifying the applications of geophysical techniques in the investigation of groundwater contamination from tanneries and slaughterhouses near Mojo River, Main Ethiopian Rift, Ethiopia. Integrated geophysical surveys involving Vertical Electrical Sounding (VES) and magnetic surveys have been used for the purpose. The VES results show the presence of intermediate to low resistivity sand clay horizons for some areas of the study, and for the others the dominant rock units are slightly fractured trachyte the same as for the most part of the area. The second layers mapped are low resistivity compact Tuff: yellowish, highly weathered trachyte and/or highly weathered and fractured basalt underlain by highly weathered bedrocks and a number of vertical or near-vertical discontinuities and weak zones in the area. The magnetic anomaly plots have mapped a number of weak zones resulting from subsurface structures. The correlation of the 2D magnetic modeling and 2D electrical resistivity or geoelectrical sections are used for the identification of weak zones that are the likely determining areas for the transfer of contaminated/wastewater to the groundwater system over the area. The work draws attention to the viability of the use of vertical electrical sounding and magnetic surveys in the identification of formations susceptible to groundwater contamination by the cause of contaminated water released from the tanneries around the Mojo area and flow downstream following the river course.

Keywords: Groundwater pollution, geophysical techniques**,** geoelectric section, magnetic anomaly, geological structures.

Acknowledgment

I would like to express my special thanks and gratitude to my thesis advisor **Prof. Tigistu Haile**, for his critical advice, inspiring guidance and encouragement throughout my research for this work. His expert advice from title selection up-to final write up of this thesis and especially for his patience and guidance during data collection from the study area, during the writing process, insightful discussion, for his support during the whole period of the study and I came to know many new things so I am very thankful to him.

I would like to acknowledge **Dr. Tilahun Azagegn**, who is a Hydrogeologist at Addis Ababa University, for providing me with information about the survey line and selection of the survey profiles over the study area. He was gone with me and we see the study area to identify the survey lines and the location of the sounding points. I am extremely grateful for his assistance suggestion and guidance during survey line profile identification.

I would like to extend my sincere gratitude to the **Ministry of Education**, for giving me the chance for an MSc degree study and the **Geology Survey of Ethiopia**, **Ethiopian Geospatial Information**, for their assistance in providing me the necessary data of hydrogeological information, topo-map respectively for the study area.

I cannot finish without thanking my family. I warmly thank and appreciate my husband for encouragement and spiritual support in all aspects.

I cannot forget to say thanks to my classmate student for continuously helping me during data collection in a very complex time, especially **Wubamlak Nigussie**, **Esubalew Yehualaw**, **Wubayehu Dessalegn**, and **Tewdros Misganaw** and the others who are numerous to mention their name here.

I would like to express my sincere gratitude to **Dr. Addis Eshetu** who is helped me to draw Magnetic 2D modeling and **Mr. Seyoum Nuguse** who is helped bring Magnetic instrument and collected data with me during data collection.

Lastly, but not list I would like to say thanks to the people who live in Mojo town and around the study area to cooperate with me during data collection with full interest.

Table of Contents

List of figures

Abbreviations

WHO	**W**orld **H**ealth **O**rganization
FOG	**F**at, **O**il, and **G**rease
COD	**C**hemical Oxygen **D**emand
BOD	**B**iological **O**xygen **D**emand
VES	**V**ertical **E**lectrical **S**ounding
ρ_a	Apparent resistivity
NMSA	**N**ational **M**eteorological **S**ervices **A**gency

CHAPTER ONE

1 INTRODUCTION

1.1 Background

Freshwater is a scarce resource, essential for agriculture, industry, human and animal life existence. Human beings, especially in developing and underdeveloped countries depend on streams and rivers to deliver much of these water use. Without adequate quantity and quality of freshwater sustainable development will not be a reality for all countries of our globe and especially so for Ethiopia. In Ethiopia, from the increasing human population and uncontrolled urbanization; improper management of the groundwater resource uncontrolled waste disposal causes serious quality degradation of the groundwater system in many areas. Now a day’s water pollution from the disposal of industrial wastewater is becoming an environmental concern in Mojo city and its vicinity areas because of the many tanneries and slaughter houses situated on its periphery and the dumping of untreated water from these industries in to the river flowing just adjacent to it- the Mojo River.

Pollution of groundwater happens mostly due to the percolation of fluvial water and the infiltration of contaminants through the soil under waste disposal sites (Abdullahi et al., 2011). Leather tanneries produce three different types of wastes, in which wastewater is the most important challenge to the environment. (a) wastewater released during in the the soaking stage (c) wastewater released during in the liming stage and (d) wastewater released during the pickling and chrome tanning. Tannery wastewater is highly polluted in terms of suspended solids, nitrogen, conductivity, sulfate, sulfide, chloride, biological oxygen demand, chemical oxygen demand, and chromium (Amanial Haile Reda, 2016).

Most often, effluents from tanning units are discharged indiscriminately into natural water bodies or open lands, resulting in contamination of the surface and ground waters. Discharges of untreated wastewater to the aquatic environment can result in the accumulation of pollutants. The consequence of this accumulation could result in loss of livelihood, loss of biodiversity, and degradation of water quality, which in general affect the ecosystem. Tanneries have been found to discharge not only Cr which, is an inherent product of the tanning process, but also significant amounts of Zn, Mn, Cu Cd, Pb, As, Ni, B, Se, Mo, N, and P have also been observed at the main waste disposal points exceeding the toxic range in soils Heavy metals (Pb, Cd, Hg, and As) contamination in drinking-water is also seriously threats human health at different levels of diseases (Amanial Haile Reda,2015).

In developing countries, such as Ethiopia, it is necessary to develop efficient waste management systems due to increased waste production as a consequence of population growth (Yazdani et al., 2015). In general, a large volume of wastes are generated daily from industries, residential and institutional environments and this can lead to dangerous diseases of epidemic magnitude if the waste is not properly disposed of. Improper disposal of these wastes can lead to groundwater pollution due to contamination by rainwater that leaches into groundwater as leachate from open dumps and sanitary landfills that usually contains both biological and chemical constituents (Olubanji et al., 2013).

River and water reservoir quality can be affected by pollution from point sources and non-point sources. Point sources are identifiable locations (such as a factory, often with a pipe or channel leading from them) that discharge directly into a body of surface water. Groundwater is also affected by point sources where contaminants seep into the soil and rock from an identifiable source, for example, underground fuel tanks, septic tanks or pit latrines. Municipal and industrial discharge pipes are good examples of point sources. Non-point or diffuse sources are those where pollution arises over a wide area and it is often difficult to locate the exact place of origin and also difficult to manage and control. ‘For example, fertilizer or pesticide that has been widely spread may be washed from a field by rain into a river or stream at many places, or seep into groundwater ‘(Yohannes H and Elias E, 2017). This is also the case when wastewater from industries, tanneries and slaughterhouses are directly pumped into a river system and the pollutants seep into the formations from areas along the river course. The subject of this study pollution of Mojo River from the tanneries and the consequent pollution of the groundwater system over the course of the river lies in this category.

Geophysical methods can be successfully used both before waste disposal operations for evaluation of site characteristics and for monitoring of possible leachate flow after dumping of the waste (Oyedran et al., 2011). The integrated use of geophysical methods provides an important tool in the evaluation and characterization of contaminants generated by urban residues (domestic and/or industrial). Geo-electric, electromagnetic, magnetic, and ground-penetrating radar geophysical techniques can, for example, effectively be applied in landfill investigations because dissolved plume (leachate) can influence resistivity /conductivity, dielectric constant, chargeability, and magnetic susceptibility of subsurface formations. Specifically, the use of geo-electrical and magnetic methods applied to landfills studies are well documented. This work aims to apply these techniques to investigate the impact of effluent from tanneries and slaughterhouses around Mojo town on the groundwater system of the area downstream of Mojo River. This research project was selected based on personal interest.

1.2 Description of the study area

The survey area is located in an area adjacent to Mojo town and covers an area of about 686km^2. Mojo town is the administrative center of Lomie Woreda and is located in the East Shewa Zone of the Oromia Regional State and is 73 km southeast of Addis Ababa where the Addis Ababa-Adama and Addis Ababa-Hawassa roads split. Is the area's landscape is primarily composed of an undulating terrain within which the elevation varies between 1788-1825 meters above mean sea level. The project area is geographically bounded between $39^{\circ}07'00''$ longitude and $8^{\circ}36'00''$ latitude. The perennial Mojo River flows adjacent to the town and, owing to the large demands and large discharge volume of used waters that emanate from the many tanneries and slaughterhouses located on its banks, factory effluent are discharged untreated or with various levels of treatment into the river system. Downstream Mojo River drains into Koka reservoir and as it enters into the large water body, it meets River Awash. Figure 1-1 gives the general location of the study area and some important landmarks in the surrounding areas.

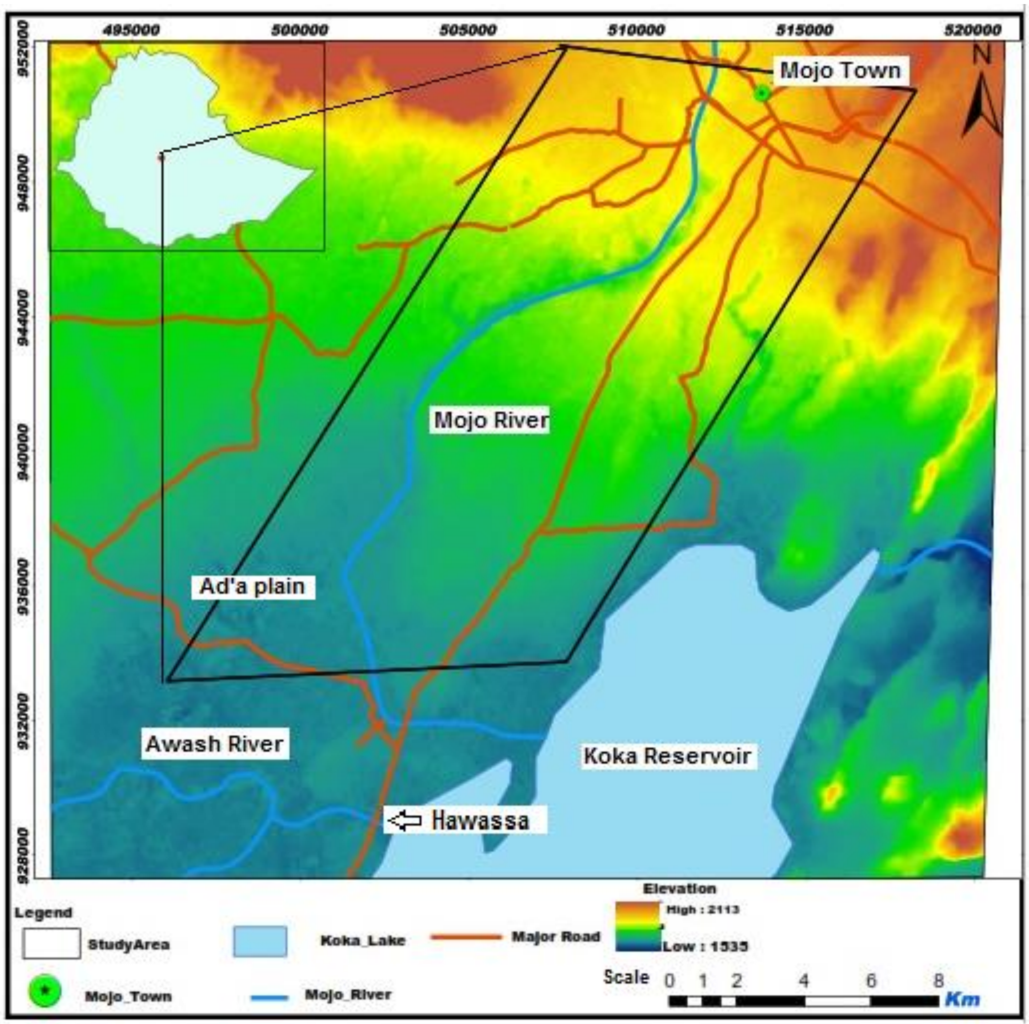

Figure 1-1 Location map of the study area.

1.3 Statement of the problem

Expansion of tannery industries and slaughterhouses along the Mojo River and discharge of untreated or partially treated tannery wastewater to the water bodies pose greater health risks to the groundwater users and ecological degradation in the water bodies. Many people that are dependent on the groundwater and river water for a variety of purposes such as drinking, fishing, livestock watering, and irrigation downstream of the river could, in due course, face shortages of clean water due to the pollution of the river and the groundwater system. The use of groundwater and the river water itself for such purposes would becomes a serious health problem. Moreover, any farming activity using groundwater containing high levels of toxic compounds (such as Cr, and other heavy metals) further exacerbate the problem.

High levels of Cr, nitrogen, and sulfur compounds in tannery industrial effluents released into the environment are problematic: for example, according to the WHO, sanitary standards for drinking water quality limit sulfate concentration less than 250 mg/l for various reasons: (i) nutrients can cause high oxygen demand and eutrophication in water bodies; and (ii) Cr contaminants cause serious health and environmental concerns; such as skin rashes, upset stomachs and ulcers, respiratory problems, weakened immune systems, kidney and liver damage, alteration of genetic material, lung cancer and ultimately death (Wang and Zhang, 2019).

Therefore, to protect the receiving environment, these contaminants should be removed from the wastewater before discharging into the environment otherwise it is a danger for the environment. This means untreated wastewater which has contaminants can easily enter into groundwater system. The problem has now forced the Ethiopian government to set discharge limit standards which demand that industries treat their wastewater before discharging them out of their setting. The government also forces the industry owners to build a treatment system that can treat the pollutants until they meet the permissible limits. It is clear that quite a number of tanneries and slaughter houses lying on Mojo River bank have non-functional treatment schemes and discharge their effluents directly into the river at odd times and the effects of their effluents are already apparent on cattle drinking water from the river in the form of blood stained urine, and in the form of skin rashes on a people dredging sand from the river bed almost at every place downstream of the tanneries. There is also a clear blackening, greasy appearance and discoloration of the river water. Mindful of these effects, the population has almost stopped using the river water for any purpose especially during the dry seasons. Therefore, the problem planned to be addressed in this research work is to assess if the impacts of the effluents from tanneries and slaughterhouses, already clearly observed to affect the livelihood and many aspects of life of the population, has already entered into the groundwater systems of the areas downstream of the town until the river discharges into Koka Reservoir.

1.4 Literature review

According to Kebede Amenu (2013) the rank of the population in the downstream of Mojo River (Koka-Nagawo and Malmale) poor water quality as the second most important problem for livestock husbandry. In this work two abattoirs and five tanneries were present at the time of the survey based on prepared questionnaire' (July2010). Most of the tanneries were discharging huge amounts of untreated wastes directly to the river. Groundwater chemistry of Mojo and its surrounding was found to be affected by urban sewage and fertilizers used for agricultural production (Kawo and Karuppannan, 2018) and in addition by effluents emanating from the industries. According to Berehanu (2007), groundwater abstraction wells located along and close to the Mojo River are very much polluted. Pollution of many folds from the acceptable limits occur due to discharging wastewater from tanneries and slaughterhouses around Mojo town directly in to the river water system (Abrha et al., 2015**).** According to Amanial Haile Reda (2016), downstream of the river is polluted as a result of the direct discharge of the tannery effluents to it as a result of the study of physicochemical parameters of Mojo River. Another idea mentioned regarding the content of trace metals from Mojo tannery effluents into the surrounding river water and soil is maximum for Cr and Cd, implying that the groundwater system is highly polluted (Amanial Haile Reda,2015). It is found however, that no geophysical surveys, however been conducted with a view to addressing this particular problem.

1.5 Objectives of the Study

1.5.1 General Objective

The main objective of this research is to employ integrated geophysical techniques for identifying groundwater contamination of downstream of Mojo River due to effluent from tanneries and slaughterhouses around Mojo town.

1.5.2 Specific Objectives

Under the umbrella of the above general objective the following specific objectives are expected to be undertaken in the present study:

- To map the subsurface geology and geologic structures over the area of the study using integrated geophysical techniques.

- Examine these geological conditions in a view of their suitability for potential pollutant transfer from the river to the groundwater system.
- To map the potential spread of the contamination in to the subsurface and specifically in to the groundwater system of the study area.

1.6 Significance of the study

Groundwater is an essential resource. It exists nearly everywhere under the Ethiopian landscape and is vitally connected to the rich surface water resources. The contamination of groundwater is a serious problem in Ethiopia. Industrial activities are major sources of contaminants. Groundwater moves so slowly that problems take a long time to appear. Because of this, and because it is so expensive to clean up once the aquifer is contaminated (if it can be done at all), it is preferable by far to prevent contamination from happening in the first place. Once these contaminants are in the groundwater, they eventually reach rivers and lakes. In other words, once such a pollution problem, exist, one may be only a step away from a water supply problem for all activities: drinking water for humans and cattle, water for agriculture and industries, etc. This might be the case where a number of tanneries and slaughterhouses located on an area adjacent to Mojo River and discharge their effluents into it.

The findings of this study, therefore, will benefit the population in the area considering that groundwater plays an important role in the livelihood of the population of an area where municipal water supplies are not accessible and the surface and groundwater is potentially exposed to pollution. In general, this proposed research will address a real problem that has potentially caused and is likely to continuously cause overwhelming damages to the population, livestock, and agricultural schemes found in areas adjacent to Mojo River on the downstream side of the tannery and slaughterhouse industries. It will help uncover critical areas of impact of the effluent from tanneries and slaughterhouses on the groundwater and considering an issue: that may have not been addressed before, specially using the techniques of geophysical exploration.

1.7 Materials and Methods

1.7.1 Electrical methods

Electrical resistivity and magnetic surveys are planned to be employed for research work. In resistivity surveying, a known amount of current (I) is pumped to energize the subsurface using a pair of current electrodes and the response is measured on the ground surface in the form of a voltage/potential difference (ΔV) through other pairs of potential electrodes. The instrument used is PASI 16 GL Earth Resistivity Meter instrument (https://pasisrl.en.ecplaza.net/products/earth-resistivity-meter-16gl-n_2573848). Resistance ($\Delta V/I$) is calculated and further, the apparent resistivity is computed by the formula $\rho_a = Kx\ (\Delta V/I)$, where K is a parameter called the geometrical factor and depends upon the way the four electrodes are put on the ground. The proposed technique for the present study is the Schlumberger array which has the strongest signal strength for a comprehensive subsurface picture. In the case of sounding (VES), apparent resistivity is obtained at a particular place by increasing the electrode separations, and the data is quantitatively interpreted in terms of layer parameters i.e. resistivity (ρ_i) and thickness (hi) of the different layers of the subsurface

1.7.2 Magnetic methods

The other method that was used is the magnetic method. This method is useful to investigate subsurface geology and specifically map contacts between different lithologies as well as subsurface structures, and weak zones on the basis of the anomalies in the Earth's magnetic field resulting from the magnetic properties of the underlying rocks. The instrument used is Proton Precession Magnetometer -600, integrated geo instruments and services plc. India. In general, the magnetic content (susceptibility) of rocks is extremely variable depending on the type of rock and the environment it is in. Common causes of magnetic anomalies include differences in rock type and dikes, faults, and lava flows. This surveys technique was conducted especially in areas where geologic structures are expected to play a role in fluid transport.

1.8 Methodology

In general, the methodology used in this study followed the stages of pre-field work, fieldwork, and post fieldwork and these are briefly described as follows:

1.8.1 Pre-field Work

In this stage of the research work, the literature on the impacts of the effluents from tanneries and slaughterhouses on the lower reaches of Mojo River, Central Main Ethiopia Rift as well as material on similar works carried out elsewhere had been assessing and reviewed as much as possible. Moreover, existing geological, as well as structural maps were reviewed, Hydrogeological, hydrometeorological, and related materials on the Mojo area in particular and Central Main Ethiopian Rift (CMER) in general to be had collected and reviewed. This study has been used to design the geophysical field campaign determine the methodologies to be used, the areas/traverses for the survey and their spacing, the data volume, etc. which is to follow in the next stage.

1.8.2 Field Work

At this stage, primary data was collected in the field by applying the geophysical methods (VES and Magnetic methods) selected for the study. By using these methods the data were collected over selected areas and transects on the project site that could be analyzed and interpreted to achieve the objectives set out in the research.

1.8.3 Post field Work

Some of the works performed at this stage are geophysical data processing using different software, interpretation of the processed data and finalization of the work The software used in electrical data analysis include RESIX, RESX IP, WinResist, Surfer and AutoCAD, while those used for magnetic data analysis are the Excel and Oasis montage. The ArcGIS software has been used for the purposes mapping the general and the local geology of the study area are along with the hydrogeological map sheet collected from the Ethiopian Institute of Geological Survey (EIGS). The overall schematic of the research methodology is depicted in Figure 1-2.

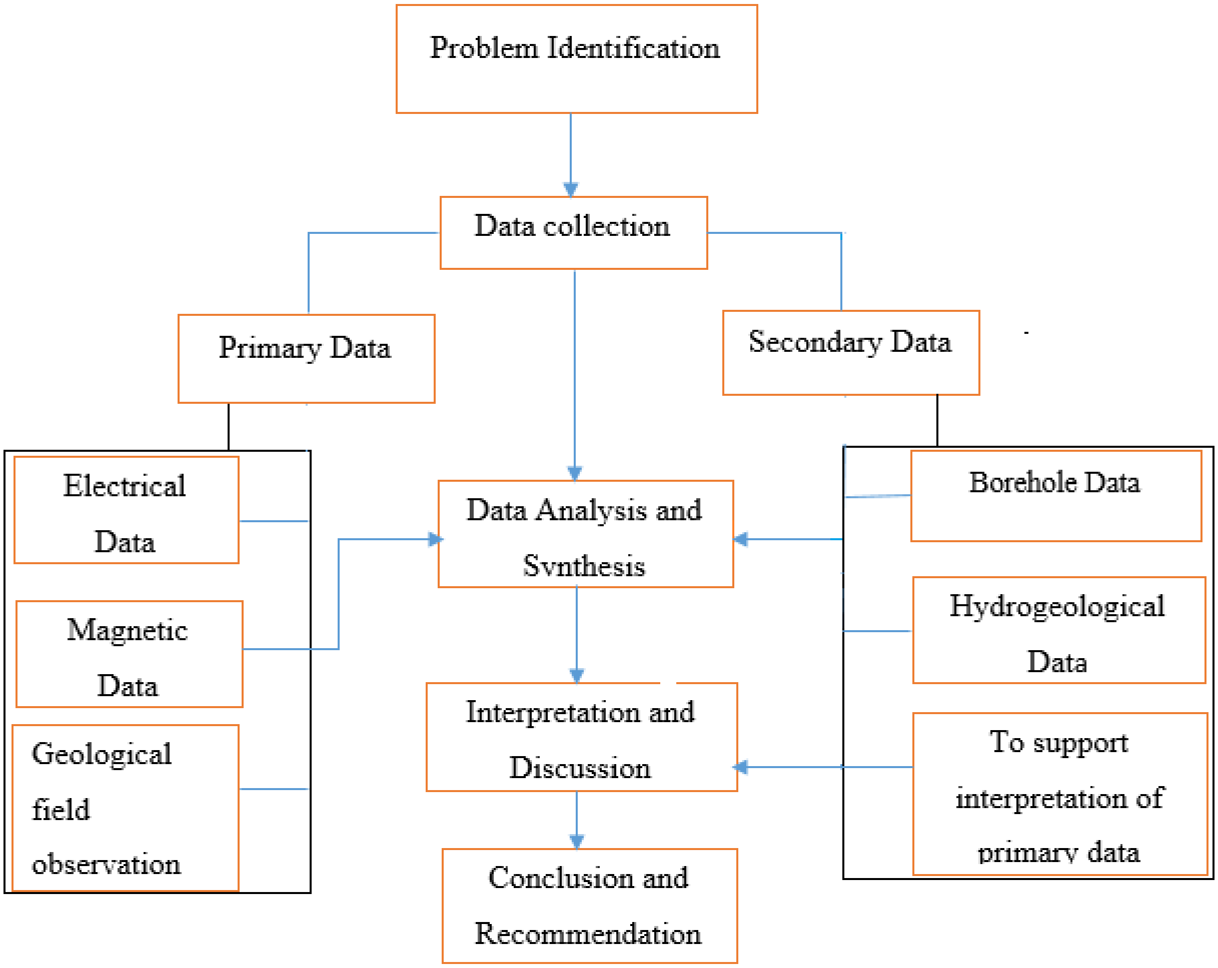

Figure 1-2 Overall framework of the research.

1.9 Hydro-meteorology

1.9.1 Climate

The study area, which is about 73km from Addis Ababa, is seen as related to areas near the equator with hot and humid climate and rain related to the general Earth's equatorial weather conditions. The weather condition of Ethiopia is basically determined by not only on its location relative to Earth's latitude but also on topography with most parts of the country being covered by high altitude terrain mostly above 2000m above mean sea level. Areas of the rift floor or its adjacent margins are characterized by elevation of more than 1000-1400m above mean sea level. Climate leads and controls soil beginning or creation, which in turn influences plant growth either positively or negatively. Different weather-related elements of the study area are summarized using the data received from the National Meteorological Services Agency (NMSA) are listed as the follows.

1.9.2 Temperature

The mean monthly temperature is taken from the data for about 30 years for some stations in the study area.

Referring to the National Meteorological Services Agency, the study area has an average temperature of 20.4℃ with the lowest possible temperature of 11.6℃ and the highest possible temperature of 29.2℃. Maximum temperature values were gotten in the months of May and the lowest possible temperature were recorded in the month of August. It is generally true that, on the average, temperature decreases with an increase in altitude. The monthly mean lowest possible temperature for Mojo station ranges from 8.5℃ to 13.5℃, with the lowest being recorded in the month of December. The monthly mean highest possible temperature for Mojo station ranges from 25.6℃ - 30.8℃whereas the highest temperature is being recorded in the month of May and the lowest in August.

1.9.3 Wind speed

In the study area, data on monthly mean wind speed at 2 meter is available only for the nearby Adama Meteorological station. In the same way, the mean monthly wind speed of the area measured at two meters above the ground changes from 1.8 to 3.5m/s with maximum values watched in the months of January and December and minimum values in the months of September and October.

1.10 Structure of the thesis

This thesis is divided into six chapters. The first chapter deals with the general statement on the problem, the objectives of the work and the methodological approach. The second chapter is concerned mostly with the work of previous researchers that includes the discussion on geology of the study area and its surroundings. Chapter three covers the theoretical background of the geophysical methods employed in this study. Chapter four describes the complete survey procedure, data acquisition, data processing, and presentation of the different results. Chapter five covers integration of the results, discussion, and interpretations of the geophysical methods. The last chapter contains conclusions and recommendations derived from the research work.

CHAPTER TWO

2 GEOLOGIC AND TECTONIC SETTING

2.1 Regional geology

The geological and geomorphologic features of the region are the result of Cenozoic volcano-tectonic and sedimentation processes and some patchy Precambrian outcrops at the southern and northern edges where, the rift is covered with Cenozoic volcanic and sedimentary rocks. The formation of the rift is associated with extensive volcanism. In many places the volcanic products were fissural basaltic lava flows, stacked one over the other, alternating with volcano-clastic deposits derived from tuff, ignimbrite, and volcanic ash (Tenalem Ayenew, 2007).Along the rift margins, most geological sections are dominated by Tertiary volcanic rocks and on a few locations where the crystalline basement is uncomfortably overlain by Mesozoic sedimentary and tertiary volcanic rocks (Giday Woldegabriel et al., 1990).

In the Ethiopian rift valley, the Nazret sheet is the middle one and covers the western and eastern parts of the highlands/escarpments and is covered by Tertiary and Quaternary volcanic rocks, lacustrine sediments and alluvium. The most known aquifers in the area are the Fantale group of ignimbrites, the recent basalts, some part of the Nazret group of ignimbrites, and lacustrine sediments around Debre Zeit and alluvials in the Metahara area. Except for the lacustrine sediments around Debre Zeit area and the recent one of basalts, the other groundwater aquifers contain high salinity and fluoride (EIGS, 1984).

When considering regional structures, the rift floor and its escarpments are generally highly faulted. ‘The rift valley is distinctly separated from the plateau by a series of normal faults usually trending parallel and sub-parallel to the NNE–SSW trending rift axis’ (Tenalem Ayenew, 2007).The floor of the rift is described by a persistent belt of intense and recent faulting and it isa tectonically active region characterized by numerous geothermal manifestations and caldera volcanoes. The faults are not evenly distributed over the rift floor but tend to be concentrated in bands. The most prominent of these bands, in this part of the rift, runs close to its eastern side and is known as the Wonji Fault Belt (WFB) system of faults (Williams, 2016). WFB faults are of normal type and are up thrown both to the northwest and southeast (EIGS, 1984).

2.2 Geology of the study area and its surroundings

According to the Ethiopian Institute of Geological Survey (EIGS) map (EIGS, 1987) at a scale of 1:25,000 the area of study for this research falls in the geology map of Nazret sheet area. From this map, one the geology of Lomie Woreda including the region up to Lake Koka. can consider different geology of Lomie woreda or my study area up to Lake Koka. The prominent units in the area are: -volcanic rocks and volcanic sedimentary deposits (consisting of alluvial cover and lacustrine sequences) as seen on the geological map of the study area that modified with the help of ArcGIS software from a geological map of the Northern Main Ethiopian Rift that was taken from the Geological survey of Ethiopia that depicted in Figure 2-1.

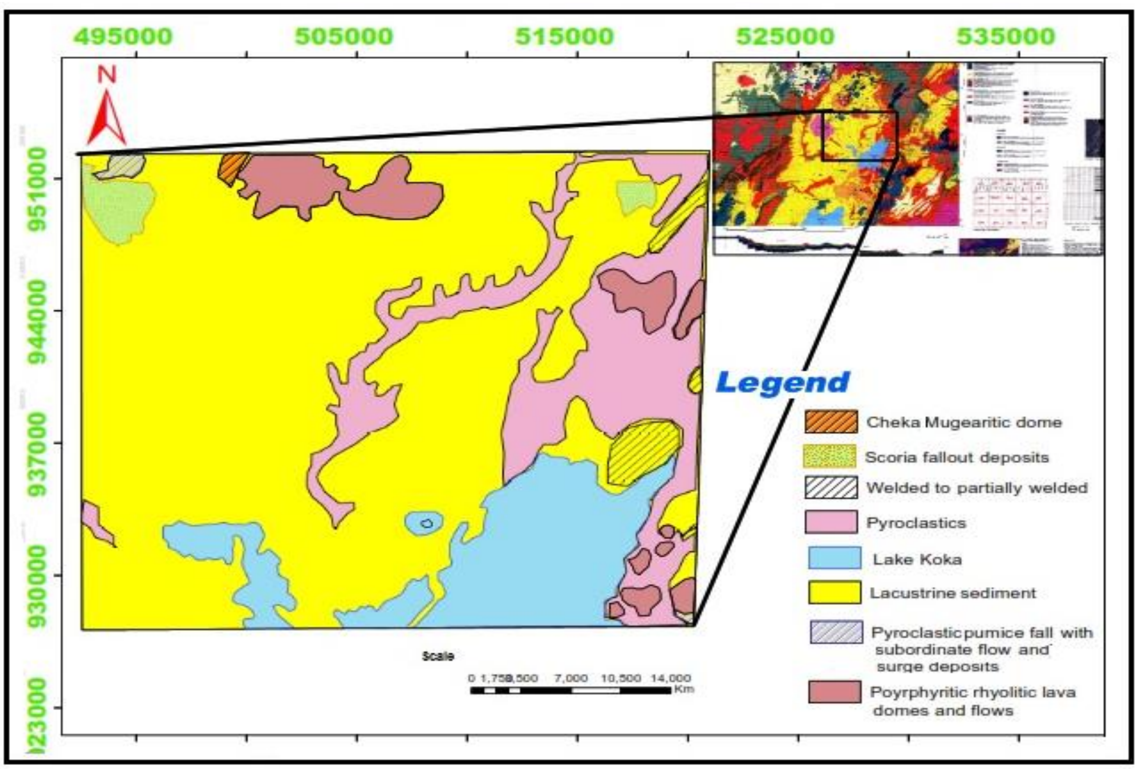

Figure 2-1 Geology of the study area (modified from EIGS, 1987)

In Mojo area, the lacustrine sediments cover the area between about 8 kilometers northwest of Mojo town and the northern part of Koka Lake, extending southwest along the Shashamene to Hawassa road up to a few kilometers south of Goriya Mountain (Figure 2-1). The estimated permeability of this rock unit from bore wells data is found to vary from 0.54 up to 2.62m/day. These lacustrine sediments in the Mojo area are grading from fine to medium-grained sand from the surface downward. The medium-grained sand is the main aquifer in the area and it is grouped as an aquifer of moderate permeability (EIGS, 1987). The water-bearing unit in the Mojo river basin are the lacustrine deposits, Quaternary scoriaceous basalts, fractured ignimbrites and fractured basalts (Kawo and Karuppannan, 2018).It is reported that these three are the important aquifer systems, namely, the Quaternary alluvial and lacustrine unit, the upper basaltic and lower basaltic aquifer unit in the Mojo river basin'. The alluvial and lacustrine aquifers exist in the flat parts of the basin and are known to have high groundwater potential.

CHAPTER THREE

3 THEORETICAL BACKGROUND OF THE METHODS OF INVESTIGATION

3.1 The Direct Current (DC) resistivity method

Direct current (DC) resistivity methods use artificial sources of current to produce an electrical potential field in the ground. In almost all resistivity methods, a current is introduced into the ground through point electrodes (C_1, C_2) and the potential field is measured using two other electrodes (the potential electrodes P_1 and P_2), as shown in Figure 3-1. The source of current can be direct current or low-frequency (0.1 – 30 Hz) alternating current. The aim of generating and measuring the electrical potential field is to determine the spatial resistivity distribution (or its reciprocal - conductivity) in the ground. As the potential between P_1 and P_2, the current introduced through C_1 and C_2, and the electrode configuration are known, the resistivity of the ground can be determined; and this is referred to as the "apparent resistivity"(Knödel et al.,2007).

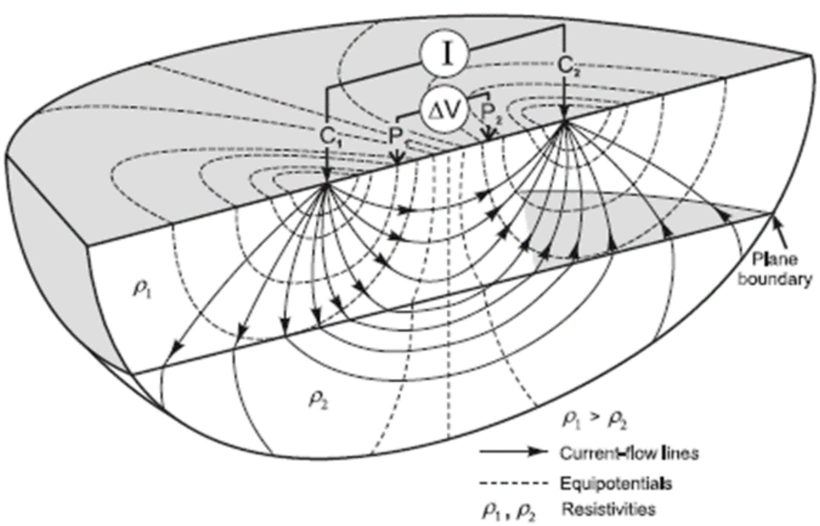

Figure 3-1Principle of resistivity measurement with a four-electrode array (Knödel et al., 2007).

3.1.1 Fundamentals of Direct Current Flow

The purpose of electrical surveys is to determine the subsurface resistivity distribution by making measurements on the ground surface. From these measurements, the true resistivity of the subsurface can be estimated. The ground resistivity is related to various geological parameters such as the mineral and fluid content, porosity, and degree of water saturation in the rock.

The fundamental physical law used in resistivity surveys is Ohm's law, a law that governs the flow of current in the ground. The equation for Ohm's law in vector form for current flow in a continuous medium is derived based on the following steps.

If one considers a continuous flow of current in voluminous media the flow of current in the medium is based on the principles of conservation of energy, i.e.

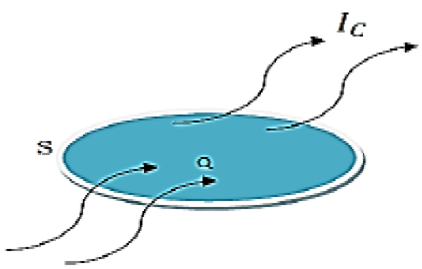

$(I_c)_s = -\frac{dQ}{dt}$,where $(I_c)_s$- is the current flow due to charges flowing out of the closed surface 's' and

Q – is charge enclosed by 's'

In terms of current density J and charge density q, $(I_c)_s$ and Q are given by

$$(I_c) = \oint \vec{J}.ds \quad (1)$$

and

$$Q = \int q.dv \quad (2)$$

where V is the volume bounded by the surface's'.

Using equations (1) and (2) in the above equation one can get the following equation.

$$\oint \vec{J}.ds = -\frac{d}{dt}\int q.dv \quad (3)$$

Applying the divergence theorem on the left hand side of the above equation, and interchanging the differentiation and integration sequence on the left hand side of the equation

$$\oint \vec{J}.ds = \int (\nabla.\vec{J}) dv \qquad (4)$$

$$\int (\nabla.\vec{J}) dv = -\int \left(\frac{\partial q}{\partial t}\right) dv$$ or

$$\int \left(\nabla.\vec{J} + \frac{\partial q}{\partial t}\right) dv = 0 \qquad (5)$$

Since equation (5) must be valid for any volume, it follows

$$\nabla \cdot \vec{J} + \frac{\partial q}{\partial t} = 0 \qquad (6)$$

Equation (6) is the law of conservation of charge in differential form, also known as the **continuity equation**.

For stationary value (i.e. direct current) $\partial q/ \partial t = 0$, then equation (6) reduces to

$$\nabla \cdot \vec{J} = 0$$

Since the stationary field is conservative, E (the electric field) may be related to the scalar vector function V as

$$E = -\nabla \cdot V$$

where V- is measured in volts.

The relation between the current density and the electric field intensity is given by Ohm's law

$$J = -\sigma \vec{E}$$

where E is measured in volts/meter and σ - is a second rank tensor in anisotropic media but it is a scalar in isotropic media and also it has a unit 'mhos' and it is the reciprocal of resistivity (ρ) 'Ωm', so one can write Ohm's law as the following:

$$= -\sigma\vec{E} = -\frac{1}{\rho}\vec{E} = -\frac{1}{\rho}(-gradV) = \frac{1}{\rho}\ gradV \qquad (7)$$

For isotropic media $\boldsymbol{\rho}$is a scalar function of the point of observation and **J** is in the same direction as E, but $\nabla.\vec{J} = 0$, so *div* $(\frac{1}{\rho}\ gradV) = 0$ this becomes

$$div\frac{1}{\rho}.gradV + \frac{1}{\rho}\ div.gradV = 0 \qquad (8)$$

Equation (8) is called **the fundamental equation of electrical prospecting** with direct current. If the medium is homogeneous, ρ is independent of the coordinate axes and equation (8) reduces to

$$div \cdot grad V = 0$$

or

$$\nabla^2 V = 0 \qquad (9)$$

which is the **Laplace Equation**.

Thus, the electrical potential distribution for direct current in a homogeneous medium satisfies the Laplace Equation. The equation has different forms in different coordinate systems:

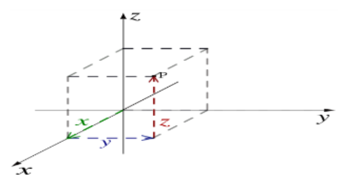

Cartesian (orthogonal) coordinate system

$$\frac{\partial^2 V}{\partial x^2} + \frac{\partial^2 V}{\partial y^2} + \frac{\partial^2 V}{\partial z^2} = 0$$

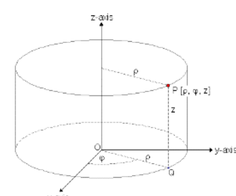

Cylindrical coordinate system

$$\frac{\partial^2 V}{\partial r^2} + \frac{1}{r}\frac{\partial V}{\partial r} + \frac{\partial^2 V}{\partial z^2} + \frac{1}{r^2}\frac{\partial^2 V}{\partial \theta^2} = 0$$

Spherical coordinate system

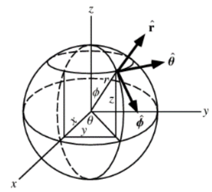

$$\frac{1}{r^2}\frac{\partial}{\partial r}\left(r^2\frac{\partial V}{\partial r}\right)+\frac{1}{r^2 sin\theta}\frac{\partial}{\partial\theta}\left(sin\theta\frac{\partial V}{\partial\theta}\right)+\frac{1}{r^2 sin^2\theta}\frac{\partial^2 V}{\partial\Phi^2}=0$$

3.1.2 Potential due to a point source on the ground

Consider the case where the point source, delivering I amperes of current, is located on the surface of homogeneous, isotropic Earth, and the air above has zero conductivity, this corresponds to a single probe or three-electrode system used in some surface resistivity measurement layouts, again the return current electrode is at a far off distance as in Figure (3-2).

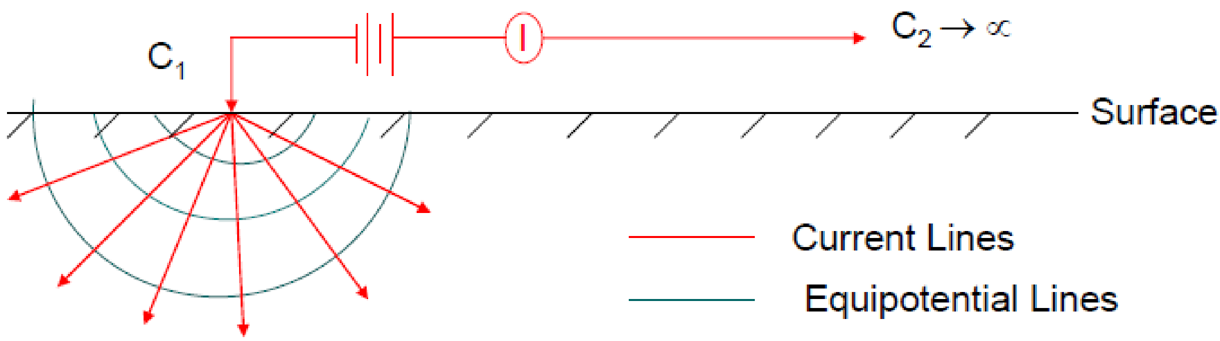

Figure 3-2 Potential due to a point source on the ground.

When one considers the above figure it is the same as the hemispherical shape and it depends on the distance (r), but it is independent of azimuthal angle (ϕ)and polar angle (θ),so that the equation of spherical shape can be reduce to

$$\frac{1}{r^2}\frac{\partial}{\partial r}(r^2\frac{\partial V}{\partial r})=0,$$

since $\frac{\partial V}{\partial\theta}$ and $\frac{\partial^2 V}{\partial\Phi^2}$ are zero.

$$r^2\frac{\partial^2 V}{\partial r^2}+2r\frac{\partial V}{\partial r}=0,$$ integrating both sides of this equation gives

$$\frac{\partial V}{\partial r} = \frac{A}{r^2} \tag{10}$$

Integrating once more

$$V = -\frac{A}{r} + B \tag{11}$$

where A and B are integration constants and can be solved by using the boundary conditions as follows: -

1. B =0 as (V →0 as r→ ∞).
2. $\frac{dV}{dz}$ = 0 at z = 0, since σ_{air} = 0, so $\frac{dV}{dz} = \frac{d}{dz}\left(\frac{-A}{r}\right) = -\frac{d}{dr}\left(\frac{A}{r}\right).\frac{dr}{dz} = \frac{Az}{r^3}$ which indeed is 0 at z = 0; so the condition $\frac{dV}{dz}$ = 0 at Z = 0 is already satisfied.
3. Further, the third boundary condition is that all the current now flows through a hemispherical surface in the lower half, so that

   I=2$\pi r^2 J$ = - 2$\pi\sigma A$, since J = -σE = -σdV/dr; dV/dr = A/r^2, so

$$A = -\frac{I\rho}{2\pi}$$

So that in this case,

$$V = \frac{I\rho}{2\pi}\left(\frac{1}{r}\right), \; or \;\; \rho = 2\pi r\left(\frac{V}{I}\right) \tag{12}$$

Here the equipotential surfaces are hemispherical below the ground as illustrated in Figure 3.2. In practice, all resistivity surveys use at least two current electrodes, a positive current and a negative current source. Figure 3.1 shows the potential distribution caused by a pair of electrodes. In practically all surveys, the potential difference between two points (normally on the ground surface) is measured. A typical arrangement with 4 electrodes is shown in Figure.3.1. The potential difference is then given by

$$V = \frac{I\rho}{2\pi}\left(\frac{1}{r_{C_1P_1}} - \frac{1}{r_{C_2P_1}} - \frac{1}{r_{C_1P_2}} + \frac{1}{r_{C_2P_2}}\right) \quad (13$$

The resistivity measurements are still made by injecting current into the ground through the two current electrodes (C_1 and C_2 in Figure 3.1.) and measuring the resulting voltage difference at two potential electrodes (P_1 and P_2). From the current (I) and potential (V) values, an apparent resistivity (ρ_a) value is calculated.

$$\rho_a = k\frac{\Delta V}{I}$$

where k = $\frac{2\pi}{\left(\frac{1}{r_{c1p1}} - \frac{1}{r_{c2p1}} - \frac{1}{r_{c1p2}} + \frac{1}{r_{c2p2}}\right)}$ is a geometric factor that depends on the arrangement of the four electrodes. Resistivity measuring instruments normally give a resistance value, R=ΔV/I, so in practice, the apparent resistivity value is calculated by

$$\rho_a = k\,R \quad (14)$$

This last of these equations are used to determine the resistivity of the subsurface by using the arrangement of the four electrodes as discussed in section 3.1 and 3.2.

3.1.3 Electrical properties of Earth materials

Earth materials include minerals, rocks, soil, and water. These are the naturally occurring materials found on Earth that constitute the raw materials upon which our global society exists. Earth materials are vital resources that provide the basic components for life, agriculture and industry. Earth materials can also include metals and precious rocks. Earth material has different properties based on one or more physical properties amongst which one the most important electrical properties of rocks. There are different types of electrical properties of Earth materials and rocks like induced polarization, resistivity; and dielectric contact i.e. the capacity of rocks to store change, that are, for example, important for mineral explorations. The nature and amount of pore saturating fluid (water, other fluids like hydrocarbon, steam; and other gases), temperature and pressure are among several important factors in determining rock electrical properties (Rahman et al., 2017).

Resistivity surveying can identify the electrical properties of rocks. Igneous and metamorphic rocks typically have high resistivity values. The resistivity of these rocks is greatly dependent on the degree of fracturing, and the percentage of the fractures filled with groundwater. So depending on whether it is wet or dry a given rock type can have a large range of resistivity, from about 1000 to 10 million Ω-m. When one compares sedimentary rocks with the other rock types, these rocks are found to have low resistivity values which are usually more porous and have higher water content and hence their resistivity values range from 10 to about 10000Ωm. in general. The resistivity of some important rocks; soils and minerals are presented in Figure 3.3.

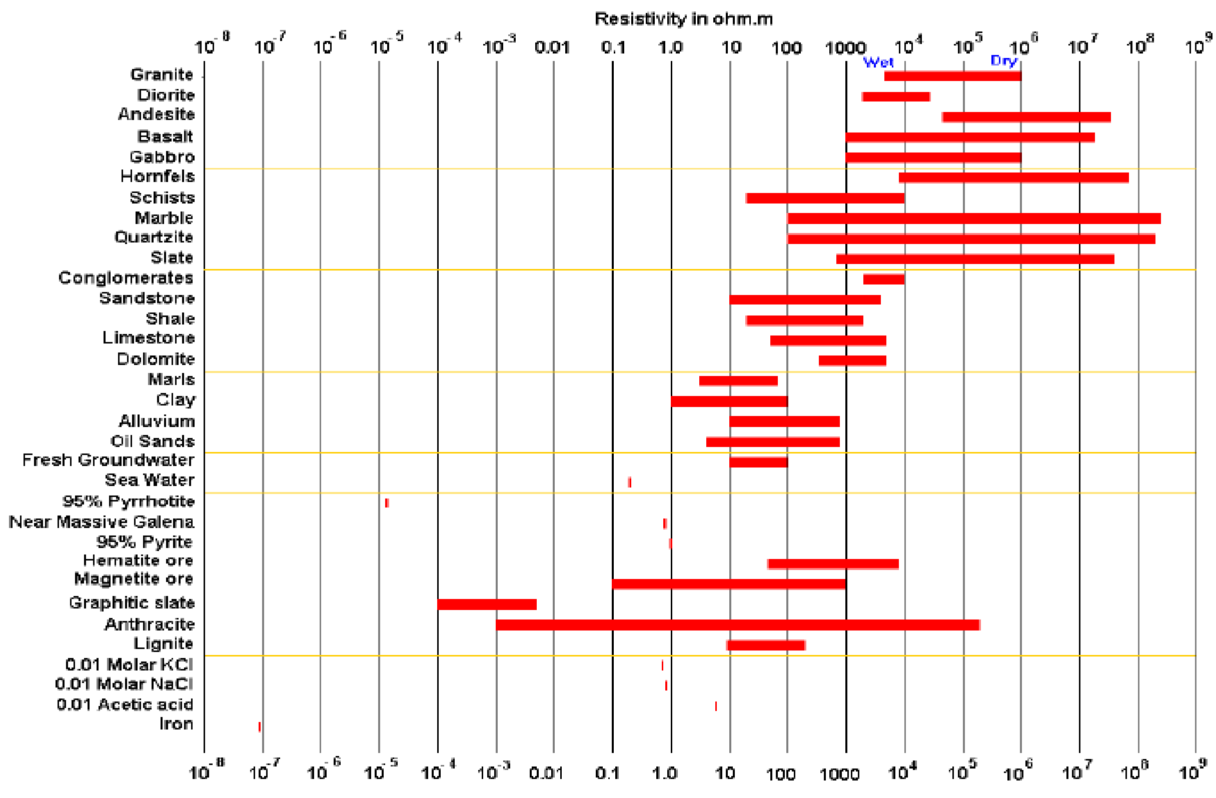

Figure 3-3. The resistivity of rocks, soils, and minerals (lecture note on the electrical method).

3.1.4 Resistivity Sounding Principle

These are procedures to determine the variations in resistivity in the vertical direction, the procedure is also known as electrical drilling or commonly Vertical Electrical Sounding (VES). It is achieved by symmetrically expanding the distance between the current electrodes about a point called the sounding point (as presented in Figure 3.1, while keeping the potential electrodes MN at the same position. This systematic increment in the separation of the electrodes during consecutive measurements; provides a sounding a curve corresponding to the apparent resistivity versus depth at the location of the sounding. As the spacing between the current electrode increases, the investigated depth will also increase.

In this thesis work, the Schlumberger array (Figure 3-4) has been used to collect the sounding data. In this system, the electrodes are symmetrically placed about a point at the center of the array (the sounding point) and increased systematically while measurements of potential and determination of the geometric parameters using the known distances between the electrodes enables the sequential determination of the apparent resistivity of the ground.

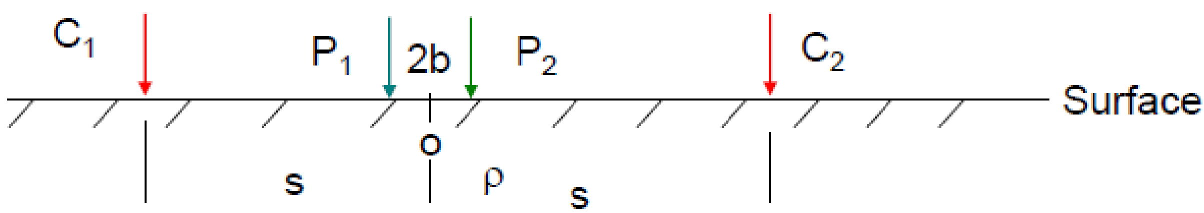

Figure 3-4 Generalized form of the Schlumberger electrode configuration in resistivity surveys to measure the subsurface resistivity.

where- $c_1 c_2 and p_1 p_2$ are two current electrodes and potential electrodes respectively and with the distance P_1P_2 much less than that of C_1C_2. The resistivity is determined from the equation.

$$\rho_a = \pi\left(\frac{s^2 - b^2}{2b}\right)\left(\frac{\Delta V}{I}\right) \tag{15}$$

where ($\pi \frac{s^2 - b^2}{2b}$) is a geometric factor and the ratio ∆V/2b is the **potential gradient** or the **intensity of the electric field**.

In electrical sounding survey, the problem is determining the depth and the electrical resistivity of a series of horizontal or nearly horizontal layers of the ground. In order to solve this problem, one should calculate the potential and the electric field, due to a point source of current; at any point on the surface of stratified Earth. To do this, there is a need to simplify the problem by first considering the potential field set up by a single point source of current. This has advantages because, it enables one to use the axial symmetry of the potential field about the vertical axis through the current source, and since potential is additive, this fact can also be used in determining the total potential from the summation of contribution from the different layers.

To work on such a problem, choose a cylindrical system of coordinate with the origin at the point source a direct current located on the surface. The subsurface consists of an infinite number of layers separated by horizontal boundary planes; the deepest layer existing to infinite depth ($h_n \rightarrow \infty$) and the other layers have a finite thickness $h_i = h_1, h_2, h_3 \dots h_n$ and each of the layers is electrically homogeneous and isotropic with resistivity$\rho_1, \rho_2, \rho_3 \dots \rho_n$ as Figure 3.5.

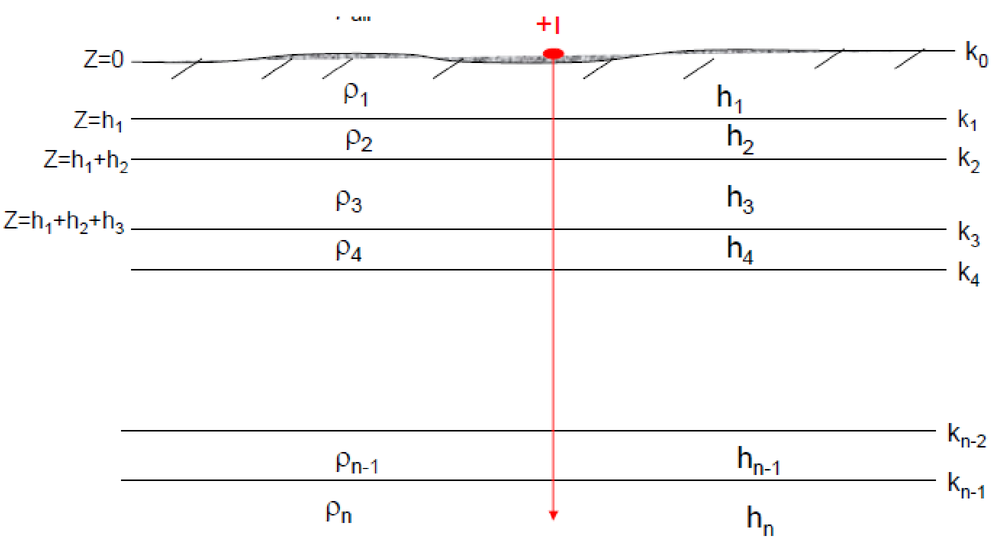

Figure 3-5Potential distribution at the surface of horizontally stratified Earth.

It is clear that the potential field has a cylindrical symmetry with respect to the vertical axis line through the current source and therefore, it appropriate to use the Laplace equation (equation 9) in cylindrical coordinate.

Hence, the electrical potential V for direct current satisfies the Laplace equation, i.e.

$$\nabla^2 V = 0 \tag{16}$$

$$\frac{\partial^2 V}{\partial x^2} + \frac{\partial^2 V}{\partial y^2} + \frac{\partial^2 V}{\partial z^2} = 0 \tag{17}$$

As stated, the potential field has a cylindrical symmetry with respect to the vertical axis/line through the current source and therefore, the Laplace Equation in cylindrical coordinates is most appropriate, i.e.

$$\frac{\partial^2 V}{\partial r^2} + \frac{1}{r}\frac{\partial V}{\partial r} + \frac{\partial^2 V}{\partial z^2} + \frac{1}{r^2}\frac{\partial^2 V}{\partial \theta^2} = 0 \tag{18}$$

For a solution symmetrical with respect to the vertical axis

$\frac{\partial^2 V}{\partial \theta^2} = 0$, so that equation (2) reduces to

$$\frac{\partial^2 V}{\partial r^2} + \frac{1}{r}\frac{\partial V}{\partial r} + \frac{\partial^2 V}{\partial z^2} = 0 \tag{19}$$

The particular solution of equation (3) can be obtained by the method of separation of variables and can be assumed to be of the form

$$V(r, z) = U(r)W(z) \tag{20}$$

Substituting equation (4) into (3) and dividing throughout by the product $U(r)W(z)$

$$\frac{1}{U(r)}\frac{d^2U(r)}{dr^2} + \frac{1}{rU(r)}\frac{dU(r)}{dr} + \frac{1}{W(z)}\frac{d^2W(z)}{dz^2} = 0 \tag{21}$$

Equation (5) is satisfied if and only if

$$\frac{1}{U(r)}\frac{d^2U(r)}{dr^2} + \frac{1}{rU(r)}\frac{dU(r)}{dr} = \lambda^2 \tag{22}$$

and

$$\frac{1}{W(z)}\frac{d^2W(z)}{dz^2} = -\lambda^2 \quad (23)$$

where- λ is an arbitrary constant. The solution of equation (23) may be given as

$$W(z) = C_1 e^{-\lambda z} \text{ and } W(z) = C_2 e^{+\lambda z} \quad (23')$$

$$U(r) = C_3 J_o(\lambda r) \quad (24)$$

where – the C's (C_1, C_2, C_3 and λ are integration constants, and

Jo is the Bessel function of order zero.

The combination of equations (23') and (24) gives the particular solution of the differential equation (23), i.e.

$$V(r,z) = C_4 e^{-\lambda z} J_o(\lambda r) \quad (25)$$

$$V(r,z) = C_5 e^{+\lambda z} J_o(\lambda r)$$

where C_4, C_5 and λ are integration constants.

Since by the theory of differential equation every linear combination of the particular solutions is also a solution of the differential equation make λ go through all possible values from $0 \rightarrow \infty$, and allow the constants C to vary independence of λ the general solution of equation (3) can be obtained as

$$V(r,z) = \int_0^\infty [\Phi(\lambda)e^{-\lambda z} + \Psi(\lambda)e^{+\lambda z}] J_o(\lambda r) d\lambda \quad (26)$$

Here $\Phi(\lambda)$ and $\Psi(\lambda)$ are arbitrary functions of λ, whose special form is determined by the boundary conditions.

From basic theory, the potential generated by a single point source of intensity 'I' located on the surface of a homogeneous Earth

$$V = \frac{I\rho}{2\pi}\left(\frac{1}{\sqrt{r^2 + z^2}}\right)$$

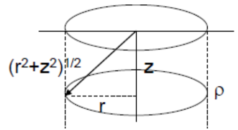

where ρ is the resistivity of the homogeneous Earth.

Equation (12) can be written in integral form using what is called the Lipchitz integral (also called the Weber integral formula) in the theory of Bessel functions as:

$$\int_0^\infty e^{-\lambda z} J_0(\lambda r)\, d\lambda = \frac{1}{\sqrt{r^2 + z^2}} \quad (27)$$

So that equation (12) gives

$$V = \frac{I\rho}{2\pi} \int_0^\infty e^{-\lambda z} J_0(\lambda r)\, d\lambda \quad (28)$$

Equation (28) is also a solution of the differential equation of equation (3).Therefore, the combined solution of equations (11) and (14) will also be a solution of (3), i.e.

$$V(r,z) = \frac{I\rho}{2\pi} \int_0^\infty \left[e^{-\lambda z} + \Theta(\lambda) e^{-\lambda z} + \mathrm{X}(\lambda) e^{+\lambda z}\right] J_0(\lambda r)\, d\lambda \quad (29)$$

where $\Theta(\lambda)$ and $\mathrm{X}(\lambda)$are arbitrary functions of λ. The solution of equation (29) is valid in all the layers of the subsurface. The functions $\Theta(\lambda)$ and $\mathrm{X}(\lambda)$are not, however, necessarily the same for the different layers of the subsurface. Therefore, the potential due to a point source of current at the surface of a horizontally layered Earth must in each layer satisfy

$$V_i(r,z) = \frac{I\rho}{2\pi} \int_0^\infty \left[e^{-\lambda z} + \Theta_i(\lambda) e^{-\lambda z} + \mathrm{X}_i(\lambda) e^{+\lambda z}\right] J_0(\lambda r)\, d\lambda \quad (30)$$

Equation (30) is called the **Stefanescu Integral** 'i' refers to the different layers of the subsurface.

Boundary conditions

For a potential set up by a single point source of current at the surface of a horizontally stratified Earth

1. At each of the boundary planes in the subsurface, the electrical potential must be the same

   $V_i = V_{i+1}$ at z = h_i

2. The vertical component of the current density must be continuous on each boundary plane (the current density normal to the boundary planes …)

   $(J_i)_N = J_{i+1}$ at z = h_i

$$\frac{1}{\rho_i}\frac{\partial V_i}{\partial z} = \frac{1}{\rho_{i+1}}\frac{\partial V_{i+1}}{\partial z} \qquad (31)$$

3. At the surface (z=0) the vertical component of the current density J_v (and hence that of the electric field intensity) must be zero everywhere except in the infinitesimal neighborhood around the current source.(in air J_{air}=0 and from condition (2), the vertical component of the current density at depth zero must be zero)
4. Near the current source the potential must not approach infinity (must remain finite) as

   $V = \frac{I\rho}{2\pi}\left(\frac{1}{\sqrt{r^2 + z^2}}\right)$ at depth 0, Z=0, as r→0

   and
5. At infinite depth, the potential must approach zero, i.e.

   $V \to 0 ... as ... z \to \infty$

Following this procedure and using the many boundary conditions, an expression for the potential (ΔV) at the surface of the stratified Earth is obtained and this, along with the measured current and the layout of electrodes on the surface are used to determine the resistivity of the subsurface for the problem given in Figure 3-5.

3.1.5 Instrumentation and field surveys

A DC resistivity survey is ultimately used to generate what is known as a ‘geoelectric’ section, which is a model of the electrical properties of the subsurface. This enables the inference of rock and fluid types as well as structure present in the subsurface where the measurements have been done. The sounding method has been extensively used to investigate the ground for resource management, such as mineral, petroleum, and groundwater resources and initially quantitative interpretation of geoelectric sounding data was conducted by using pre-computed or ‘standard’ sounding curves or 1D resistivity values (Loke et al., 2013).

In the current work, electrical sounding data has been carried out along five lines lying between Mojo town and the entrance of Mojo River into Koka reservoir. It was not possible to space the profiles regularly as there is a change in ground setting, farm land usage and habitat of the area, but the lines have been selected and spaced so as to cover the area to be surveyed as much as possible. A total of 14 sounding has been collected. The maximum half current electrode spacing (AB/2) employed is 750 m. Optimum separation between the sounding points on each line is taken to be grearthan and equal 500 m. The instrument used for the survey is the PASI 16 GL Earth Resistivity Meter with P100-3 Energizer (https://pasisrl.en.ecplaza.net/products/earth-resistivity-meter-16gl-n_2573848) along with the required accessories consisting of stainless steel electrodes, cables on reels, hammers as well as a number of connector cables. A Garmin GPS (GPS map 64s, https://garmin.com/en-US/US/p/140022) has been used for sounding point location.

3.2 Magnetic Methods

3.2.1 Basic theory of the Earth’s magnetic field

If two magnetic poles of strength $m_1$and $m_2$are separated by a distance ‘r’, a force, F, exists between them. If the poles are of the same polarity the force will push the poles apart and if they are of opposite polarity, the force is attractive and will draw the poles together. The equation for the force F is given by.

$$F = \frac{\mu_0}{4\pi} \frac{m_1 m_2}{\mu_R r^2} \tag{32}$$

where μ_0 and μ_R are respectively constants corresponding to the magnetic permeability of vacuum and the relative magnetic permeability of the medium separating the poles while 'r' is the distance between them.

The magnetic field B due to a pole of strength m at a distance 'r' from the pole is defined as the force exerted on a unit positive pole at that point (Adagunodo et al., 2015) i.e..

$$B = \frac{\mu_0}{4\pi} \frac{m}{\mu_R r} \tag{33}$$

3.2.2 Magnetic Units

The magnetic flux lines between two pole per unit area are the flux density B (and is measured in weber/m2=Tesla). B, which is also called the "magnetic induction", is a vector quantity. The use of Tesla is too large to be practical in geophysical work, so a sub-unit called a nanotesla (1nT = 10-5T) is used instead, where 1nT is numerically equivalent to 1 gamma in c.g.s. units (1nT is equivalent to 10-5 gauss).The magnetic field can also be defined in terms of a force field that is produced by electric currents.

This magnetizing field strength **H** is defined following Biot-Savant's law, as being the field strength at the center of a loop of wire of radius 'r' through which a current 'I' is flowing such that

$$H = \frac{I}{2r} \tag{34}$$

Consequently, the units of the magnetizing field strength **H** are amperes per meter (Am^{-1}). The ratio of the flux density **B** to the magnetizing field strength **H** is a constant called the absolute magnetic permeability (μ) (Adagunodo et al., 2015).

3.2.3 The Earth's Magnetic Field

The geomagnetic (Earth's magnetic) field at or near the surface of the Earth originates largely from the Earth's outer core (Figure 3.6). This field can be described in terms of the declination, D, inclination I, and the total force vector **F**. These three elements are commonly used to describe the Earth's field while all the other relevant components are derivable from these. The vertical component (that directed towards the Earth's center) of the total magnetic intensity (F) of the Earth's magnetic field varies with latitude; from a minimum of around 30,000 nT at the magnetic equator to 60,000 nT at the magnetic poles. For this and related description the direction of the ambient geomagnetic field is taken to be the direction of a freely suspended magnetic needle at any point on the surface of the Earth will settle. The total field strength is found to vary from about 25,000 nT in the equatorial regions to about 70,000 nT at the poles (Adagunodo et al., 2015). The inclination is the angle from the horizontal plane to the vector and the declination is the angle from the x-axis to the component H, which is the horizontal component of the total field vector **F**.

Another way of describing the Earth's magnetic field is by specifying **H**, the vertical component **Z**, and the declination, **D**. The equations of their internal relations are (see Figure 3-6):

F = $\sqrt{X^2 + Y^2 + Z^2}$, H = $\sqrt{X^2 + Y^2}$, I = arctan (Z/H), and D = arctan (Y/X)

The components in Cartesian coordinates are:

X =H cos(D), Y =H sin(D), Z =F sin (I).

The geomagnetic field components X, Y, Z and H are given in nanoteslas (nT)

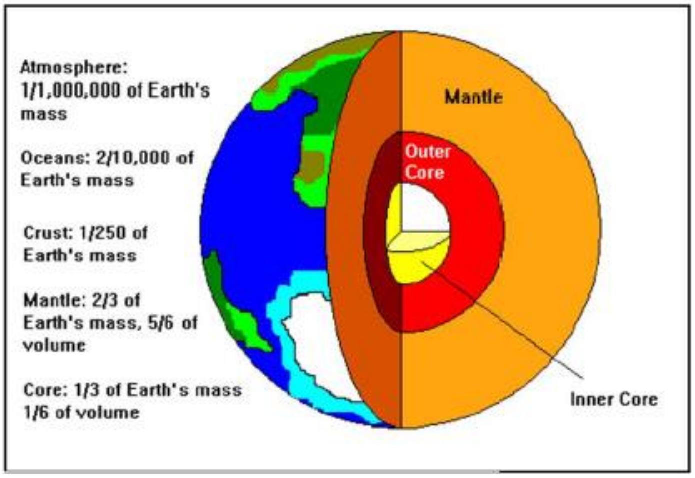

(a)

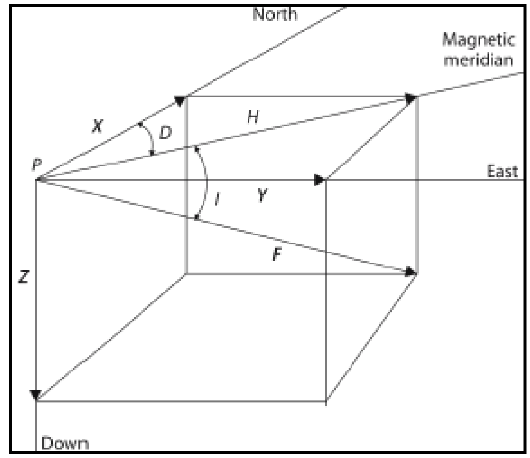

(b)

Figure 3-6 a) The overall structure of the Earth (Adagunodo et al., 2015), and .

b) the elements of the Earth's magnetic field. **F** is the total intensity of the field, **H** is the horizontal component of **F**, **D** is the declination and I the inclination (Gunnarsdóttir, 2012)

The Earth's magnetic field is divided into two, namely; the internal magnetic field and the external magnetic field. Most of the remaining small portion of the geomagnetic field appears to be associated with electric currents in the ionized layers of the atmosphere, this one is as external magnetic field and internal magnetic field has dipole field and field of rock magnetism. The strength of the field due to external sources is much weaker than that of the internal sources. Moreover, the typical time scale for changes in the intensity of the external field is much shorter than that of the field due to the internal source. Variations in the magnetic field due to an external origin (atmospheric, solar wind), called Diurnal Variations, are often on much shorter time scales so that they can be separated from the contributions of the internal sources. Generally, the total magnetic field can be expressed as to be composed of the following parts

$$B_T = B_{ext} + B_{int} = B_{ext} + B_D + B_{rm}$$

where B_{ext} is the External magnetic field, B_{int} is the internal magnetic field, B_D is the dipole field and, B_{rm} is the part of the field arising from rock magnetism

In magnetic surveys, field instruments measure the total field B_T but the survey targets are the rock magnetism B_{rm}. One therefore needs to remove the other quantities i.e B_D and B_{ext}- in a procedure called correction to obtain the value $B_{rm.}$

3.2.4 Magnetic properties of rocks and minerals

The existence of magnetic minerals in rocks causes distortion in the Earth's magnetic field. Based on the basis of magnetic properties all Earth's materials can be classified into diamagnetism, Paramagnetism, ferromagnetism, antiferromagnetic and ferrimagnetism (Adagunodo et al., 2015). 'All materials have magnetic susceptibility which can be either positive (paramagnetic) or negative (diamagnetic)' (Hunt et al., 1995).

Diamagnetism

Diamagnetism is a concept in which the field of a substance, when placed in an external field, is dominated by atoms with orbital electrons oriented to oppose the external field (Adagunodo et al., 2015).This behavior prevails only if the net magnetic moment of all the atoms is zero. Diamagnetism is a quantum mechanical effect that occurs in all materials and when this phenomena is the only contribution to the magnetism, the material is called diamagnetic. The susceptibility of diamagnetic substances is weak and negative.

Paramagnetism

When the external magnetic force is zero, materials whose moment is not zero are called paramagnetic. In paramagnetic substances, the electron shells are incomplete so that a magnetic field results from the spin of their unpaired electrons. When placed in an external magnetic field, the dipoles corresponding to the unpaired electron spins rotate to produce a field in the same sense as the applied field so that the susceptibility is positive. This is still, however, a relatively weak effect (Kearey et al., 2002).

Ferromagnetism

In ferromagnetic materials the dipoles are parallel, giving rise to a very strong spontaneous magnetization that can exist even in the absence of an external magnetic field, and such materials show very high susceptibility. Ferromagnetic substances include iron, cobalt and nickel, and rarely occur naturally in the Earth's crust. In antiferromagnetic materials such as hematite, the dipole coupling are antiparallel with equal number of dipoles in each direction. In ferrimagnetic materials such as magnetite, the dipole coupling is similarly antiparallel, but the strength of dipoles in each direction are unequal. Consequently, ferrimagnetic materials can exhibit a strong spontaneous magnetization and a high susceptibility. Virtually all the minerals responsible for the magnetic properties of common rock types fall into this category (Kearey et al., 2002).

3.2.5 Magnetic surveying instruments

There are several types, including the torsion head magnetometer and the Schmidt vertical balance, but all consist essentially of bar magnets suspended in the Earth's field. But most of these older version instruments are not sensitive enough and are also cumbersome for taking rapid measurements in the field and hence have recently been replaced by modern state of the art instrumentation derived from a better understanding of nuclear phenomena. Three of the most recent of these are discussed;

Fluxgate magnetometer

Since the 1940's, a new generation of instruments has been developed which provide virtually instantaneous readings and require only coarse orientation so that magnetic measurements can be taken on land, at sea, and in the air. These instruments employ two identical ferromagnetic cores of such high permeability that the geomagnetic field can induce a magnetization that is a substantial proportion of their saturation value. Identical primary and secondary coils are wound in opposite directions around the cores. An alternating current of 50–1000 Hz is passed through the primary coils generating an alternating magnetic field. In the absence of an external magnetic field, the cores are driven to saturation near the peak of each half-cycle of the current. The alternating magnetic field in the cores induces an alternating voltage in the secondary coils which are at a maximum when the field is changing most rapidly. The fluxgate magnetometer is a continuous reading instrument and is relatively insensitive to magnetic field gradients along the length of the cores. The instrument may be temperature sensitive, requiring correction for such effect (Kearey et al., 2002).

Proton magnetometer

Currently the most commonly used magnetometer for both survey work and observatory monitoring is the nuclear precession or proton magnetometer. The sensing device of the proton magnetometer is a container filled with a liquid rich in hydrogen atoms, such as kerosene or water, surrounded by a coil. A current is passed through the coil to generate a magnetic field Bp which normally is 50–100 times larger than the geomagnetic field, and in a different direction, causing the protons to realign in this new direction. The proton magnetometer is sensitive to acute magnetic gradients which may cause protons in different parts of the sensor to process at different rates with a consequent adverse effect on precession signal strength (Kearey et al., 2002).

Optically pumped magnetometer

Optically pumped or alkali vapor magnetometers have significantly higher precision than other types. They comprise of a glass cell containing an evaporated alkali metal such as cesium, rubidium or potassium which is energized by light of a particular wavelength (Kearey et al., 2002).

3.2.6 Magnetic surveying

Magnetic surveying can be carried out on land, at sea; and in the air. Ground magnetic surveys are usually performed over relatively small areas on a previously defined target. Readings should not be taken in the vicinity of metallic objects such as railway lines, cars, roads, fencing, houses, etc., which might perturb and, in most instances, mask the local magnetic field. For similar reasons, operators of magnetometers should not carry metallic objects and should be as magnetically clean as possible. Land surveys are usually done by portable proton precession magnetometers.

In this work the survey lines of the magnetic surveying are along the survey lines of the vertical electrical sounding surveys. In principle, these survey lines are to be chosen based on the scientific argument that it should be perpendicular to the strike of an elongate body but over the study area, this condition could not, however, be established with certainty owing to the complex geologic setting and hence, the most convenient direction for elongated survey traverse has been chosen, The next step was to select a point/points called a base station/s where readings start and end in a loop and repeat measurements are taken for the purpose of diurnal correction and to estimate the main field over the study area. In the magnetic surveying conducted over the area, the operator must: record the total field strength- with multiple readings taken at each station to check for repeatability- the time at which readings were taken for drift correction, and the location of the measuring point.

The instrument used for the magnetic survey in this work is the proton precession magnetometer (https://www.etesters.com/catalog/1273C20D-C4A0-E031-7273-357643FE89B4/integrated-geo-instruments-services-private-limited/) and position locations were determined using a hand held GPS (Garmin GPSMAP 64s).

3.2.7 Reduction of magnetic data

The reduction of magnetic data is necessary to remove all causes of magnetic variation from the observations other than those arising from the magnetic effects of the subsurface (Kearey et al., 2002). Some of the most important corrections are:

Diurnal variation correction

The effects of diurnal variation may be removed in different ways. For surveys conducted on land, the magnetometer is read at a fixed base station periodically throughout the day.The differences observed in base readings are then distributed among the readings at stations occupied during the day/or a loop defined by readings taken at the base station/ according to the time of observation. Magnetometers do not drift and base readings are taken solely to correct for temporal variation in the measured field (Kearey et al., 2002).

Geomagnetic correction for the Main Field

The geomagnetic correction removes the effect of a geomagnetic reference field from the survey data. The most rigorous method of geomagnetic correction is the use of the IGRF, which expresses the undisturbed geomagnetic field in terms of a large number of harmonics and includes temporal terms to correct for secular variation. Survey data at any given location can be corrected by subtracting the theoretical field value B_{th}, obtained from the International Geomagnetic Reference Field (IGRF) from the measured value, B_{ob}. Therefore, the magnetic anomaly (ΔB), obtained by subtracting the diurnal correction (δB_D) and geomagnetic correction (Bth) is given by

$$\Delta B = B_T - \delta B_D - Bth$$

where B_T is the total field, δB_D is diurnal correction and B_{th} is IGRF correction.

Alternatively, this correction can be effected by taking the average values of all the readings taken at the base station and subtracting it from the reading. In normal practice, readings are taken at a particular selected station repeatedly, say for a day, to establish the prevailing field value over the area by taking the average of all the readings taken. If time does not allow, repeat readings taken at the base stations can be used and are found to be adequate. In comparison, main field corrections made with averaged base station readings are more accurate that made with the IGRF value.

CHAPTER FOUR

4 DATA ACQUISITION, PROCESSING, INTERPRETATION, AND PRESENTATION

4.1Instrumentation and Data Acquisition

The electrical resistivity data were collected using the PASI 16 GL Earth Resistivity Meter instrument with P100-3 Energizer. A total of 14 Schlumberger vertical electrical sounding were carried out in an area with array spread to a maximum half current electrode spacing (AB/2) of 1000m. In the VES method of survey, the current is driven into the ground using a pair of current electrodes C_1 and C_2 and the resulting potential is measured using the two potential electrodes P_1 and P_2, (Figureb3-4).The potential electrodes remain fixed at a point while the current electrodes are expanded symmetrically about the center of the spread the sounding point. The potential electrode separations were also increased at a large value of the current electrode spread to ensure that the measured potentials are not very small. It is clear that distance between P_1 and P_2 never exceeds (AB/2) (and normally $C_1C_2 \geq$ 5 to $10P_1P_2$ where AB is the distance between current electrode. The value of the resistance is measured and the apparent resistivity calculated by multiplying the geometric factor K with the measured resistance.

Survey was done along five profiles all oriented in a near north-south and also the east-west direction with large distance/separation between the profiles so as to cover the large area and get regional interpretation of the data. Figure 4.1 gives the location of the five profiles over the survey area and Figure 4-2 gives photos showing the general field setting for the electrical (a) and magnetic (b) surveys. VES data were plotted concurrently as they are recorded to as certain data consistency and quality while repeat readings were taken to rectify any data discrepancy. Data analysis then followed using a number of software including: Surfer, WinResist and AutoCAD to interpret the VES data and present them in different form.

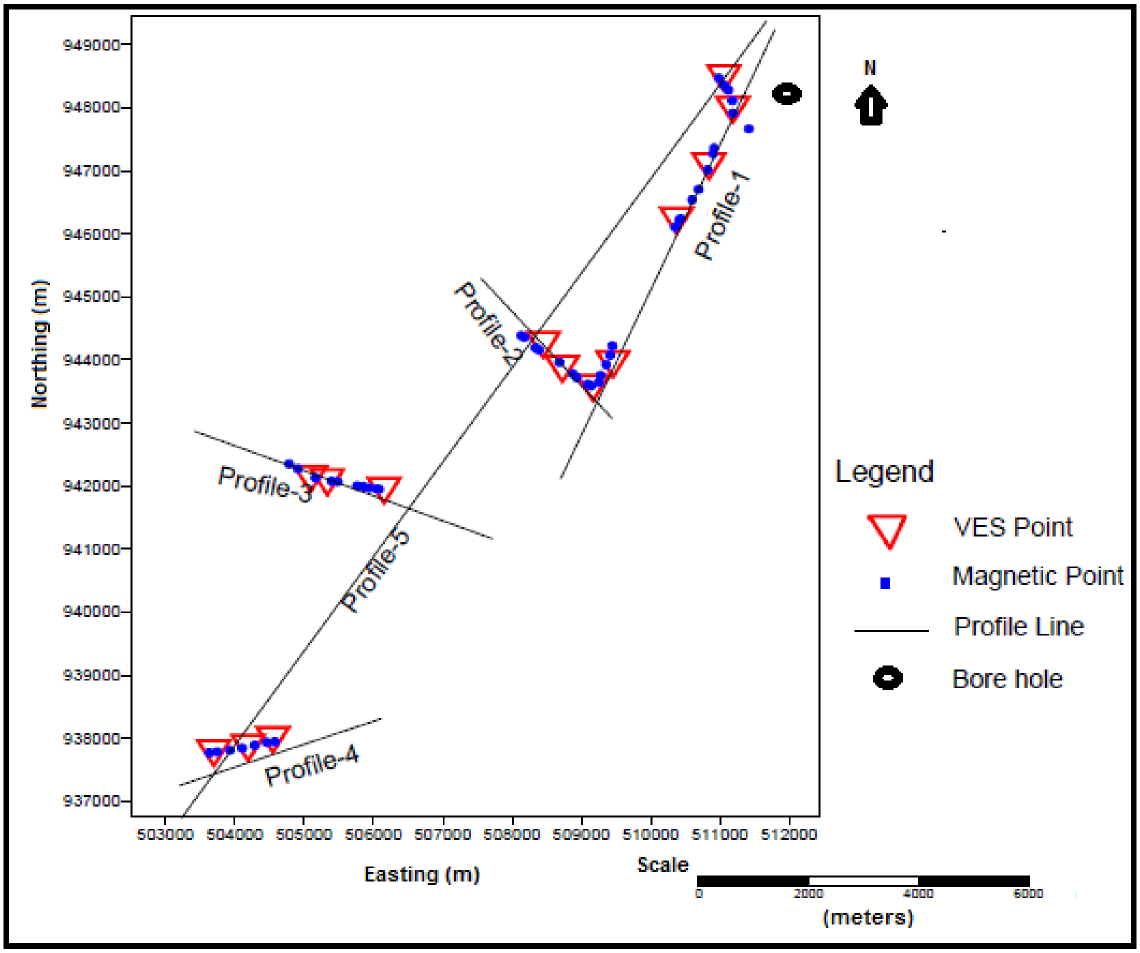

Figure 4-1 VES points (inverted triangles), magnetic survey data points (solid dots), and borehole data points (solid ellipse).

The magnetic data were collected by using Proton Precession Magnetometer -600, integrated geo instruments and services plc. India (https://www.etesters.com/catalog/1273C20D-C4A0-E031-7273-357643FE89B4/integrated-geo-instruments-services-private-limited/). over the VES profiles, but it is was difficult to collect data over random points, as planned, so as to cover the area of investigation with larger data density because the survey lines are far from each other (Figure 4-1) and the survey for regional interpretation on the groundwater potential of the area can be polluted or not based on contact zones/structures around that area. The total magnetic data collected during the field survey was 225 data points with 10 base stations. The interval reading points are 20m and the reading of magnetic anomaly at the base stations are 2 up to 3 readings. while 225 data were used for the interpretation by using the Excel spreadsheet for data filtering and diurnal correction and the Geosoft Oasis Montaj v. 6.4.2, software for data enhancement and processing. The survey points and lines for magnetic data are given in Figure 4-2, with only the sample of the data points displayed so as not to congest the plot.

Figure 4-2 Photo showing the general field condition, surface morphology and setup for the (a) electrical and (b) magnetic survey over the area.

4.2 Data Processing and Presentation

To begin with the data interpretation, first the raw data are plotted in the form of apparent resistivity pseudo depth sections for each of the profiles using the Surfer software. This is a very good representation of the VES data as it is gives an unbiased (without any data filtering or correction) view of the subsurface resistivity variation. Next, the one-dimensional modeling of individual VES data was done by using the WinResist resistivity modeling software where apparent resistivity values are converted into true resistivity and thickness of the layers beneath the sounding points. The interpreted layer parameters (resistivity ρ_i and thickness h_i of the layers) from the modeled VES are then used to construct the geoelectric sections for each survey line using the AutoCAD drawing software. A sliced-stacked map built from the apparent resistivity sections for selected (AB/2) values, were further used for a better understanding of the subsurface condition of the whole survey area. This map can show the likely groundwater saturated zones over the survey area and determine if the groundwater system is polluted considering the resistivity value and comparing it with expected resistivity response of potentially saturated rocks over the survey area.

The magnetic data were corrected first for instrumental reading errors through close examination of the data and removal of spurious readings. Next, correction was made for diurnal variation using the repeat base station readings. The magnetic data were then corrected for the main field by IGRF (OR the average value of magnetic intensity readings at the base station) then the resulting data is used to obtain the plot of magnetic anomalies. Latitude and longitude correction were insignificant and not done because the study area is found within the low latitude magnetic equator and is over a much localized area. Moreover, reduction to the pole is generally unstable and cannot be derived, so for this reason reduction to the pole was not done.

After the above corrections were done using the excel spreadsheet profile maps for each line were plotted by Geosoft Oasis Montaj v. 6.4.2 software, and further the data enhancement techniques were used to obtain a magnetic anomaly is not done because of the survey of magnetic data was collected only along profile lines that are not interconnected; because profile lines are far from each other as mentioned in the previous sections.

CHAPTER FIVE

5 RESULTS, DISCUSSIONS, AND INTERPRETATIONS

5.1 General

From the present study, interpretation of the geophysical data has been carried out to give a meaningful geological interpretation of the subsurface and examine the possibility of groundwater contamination with contaminant sources from Mojo River around the Mojo area. The interpretation of geophysical data, especially that of the electrical data, is supported by borehole data available from wells found close to the area of the study. The borehole data helped to understand the downhole and lithological-based section of the study area and correlate the different units of the geoelectrical section. The borehole data was obtained from a well drilled by Shandong Geo-mineral Engineering Company at a location close to Profile-1 with coordinates 0512300E, 0953358N at an elevation of 1785m a.m.s.l as considering from appendix-2. The depth of the borehole used for lithological correction during VES data interpretation is 358m ; whereas the depths of the geoelectrical sections are nominally about1000m.

Therefore, the relation between the well lithological log and the geoelectrical section was done only up to similar depths. The large depth than well lithological log depth of geoelectrical sections is focused on the rock resistivity value mentioned in the theory of electrical data as we follow in the above. The geoelectrical section were plotted for all profiles and discussed for each survey Profile separately. The interpretation of magnetic data and electrical data re separately mentioned as the following.

5.2 Magnetic data results

In the preceding section magnetic anomaly plots for the respective survey, lines have been presented and separately discussed (Figures 5-4, 5-7, 5-10, 5-13 and 5-16). These figures show the combined horizontal derivative of all magnetic profiles (HDR versus profile distance) over a subsurface consisting of a high magnetic susceptibility basement intruded into an overlying low-susceptibility sedimentary layer and resulted in the creation and construction of horsts and grabens. The HDR profile plot consists of HDR positive peak values (maxima) and HDR negative peak values (minima) distributed along with the profile. The HDR positive peak values (maxima) happen along edges the horsts. These edges mark locations of up-and-down contacts between the horsts and grabens. This hints that for near-surface bodies in near-up-and-down contacts, the maximum horizontal gradient of magnetic as measured along a profile happened straight-up-and-down above the contact pointing showing that the HDR method is designed to inspect locations of the fault and contact features along my survey lines. As we consider from all profile the maps are mag (nT) versus distance (km). As we follow all profiles maps at a different distance there are weak zones.

5.3 Vertical Electrical Sounding (VES) Results

1D modeling of VES data

All the 14 VES data are first interpreted by using the WinResist software to obtain the subsurface layer parameters i.e. the true resistivity and thickness of the different layers. The WinResist software works by using input models and matching the field data with the model and finding the best match between them through an iteration process in the least-square sense. A good match between the model and the field data and the data quality is .shown by the percentage RMS error displayed by the software.

A typical result of the 1D interpretation with the WinResist software is illustrated in Figure 5-1 while interpreted 1D models of all the 14 sounding data are included in the Appendix

Pseudo depth and Geoelectric sections for the survey profiles

General Remark

As a general remark regarding apparent resistivity pseudo depth sections and their significance in the interpretation of electrical resistivity data is that these representation of resistivity data provide, as mentioned elsewhere in this work, an unbiased look into the data set by using a color plotting presentation. In order to identify the resistivity value from the pseudo depth section, the map was drawn by surfer software as ones consider from the following modeling. As we see the value of resistivity from the pseudo depth section some parts of modeling show there is low resistivity less than 10Ωm. This identify there is groundwater contamination around that area. That means as we follow the value of rock resistivity listed from the above theory of electrical method the resistivity value of contamination of groundwater is less than ten, so based on this idea we can interpret the pseudo depth modeling and slice stacking created based on the pseudo depth section. Most of the modeling shows at large distances there is polluted groundwater based on the resistivity value on the color bar. The slice stacking section can be used to identify the depth at which groundwater can be polluted.

.

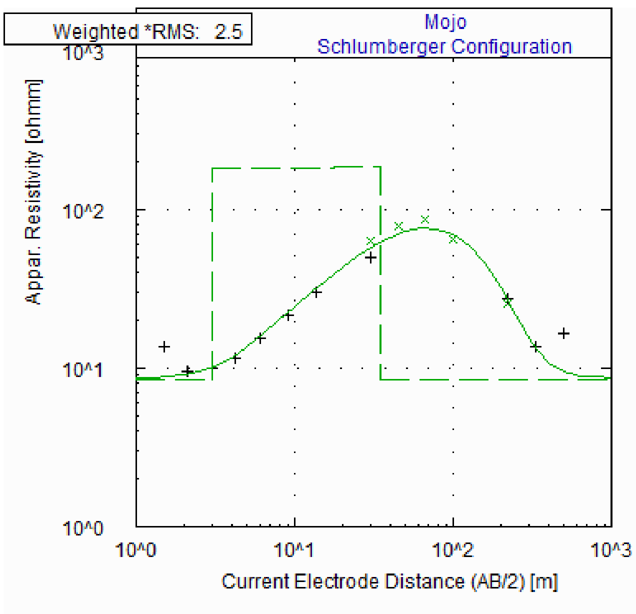

No	Res	Thick	Depth
1	8.5	3.0	3.0
2	180.8	14.7	17.7
3	188.5	16.7	34.4
4	8.5	-.-	-.-

* RMS on smoothed data

Figure 5-1Typical 1D interpretation of VES data illustrated here for VES-2 of Profile–1 (The interpreted number of layers and layer parameters are given, The RMS error indicates the degree of fit between the model and field data and it is also an indicator of data quality).

Regarding the geoelectric section, the final result from one-dimensional inversion of VES data lying along a selected profile was used to draw the geoelectrical sections in order to identify the variation of different lithological units in the up-and-down direction. The software which was used for the inversion of the VES data was WinResist then plotting of the geoelectrical section was carried out by using later modified by AutoCAD software. As we follow from the following figure the RMS-error is less than five percent (5%). The geoelectrical section of different profiles is mentioned as the following.

Profile-1

a) Pseudo-depth section

Most parts of the figure below show a low resistivity value is less than 10Ωm. These values show that the groundwater is already contaminant, because of the resistivity value of freshwater is greater than 10Ωm as consider from Figure 3-3. The cause of this contamination is wastewater released from the industries inter to the groundwater through the weak zone around the study area as illustrated by the dashed line in Figure 5-2.

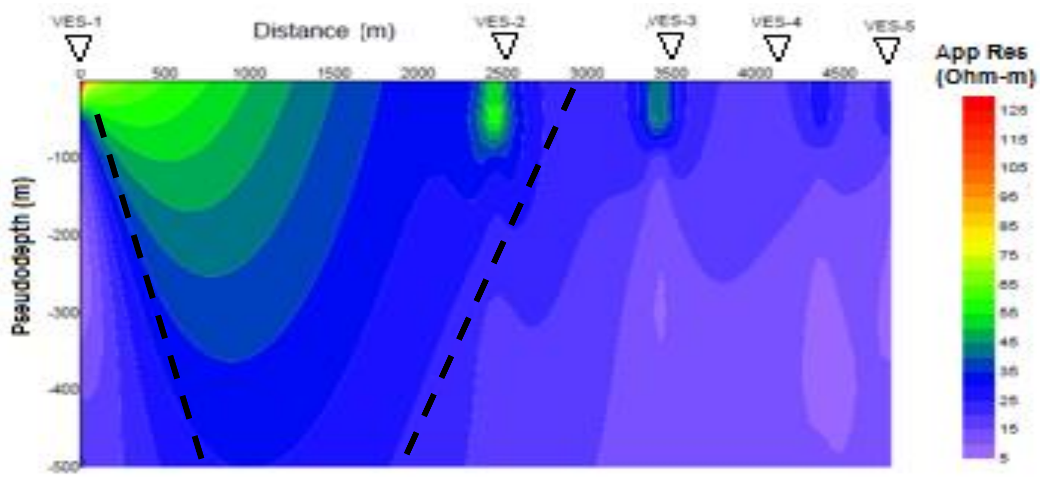

Figure 5-2 Apparent resistivities pseudo-depth section for Profile-1.

b) Geoelectric section

Figure 5-3 gives the geoelectric section constructed from the interpreted VES lying on Profile-1 and the interpretatios are depends on the appendix-2 well log data. It is seen from the plot that the first layer is the sand-clay that shows relatively low resistivity ranging from 7–9 Ω-m and extending to a depth of 3m. The second layer in the geoelectric section exhibits high resistivity values that could be due to pumic: light gray and there is a weak zone around the second layer as we consider from the bellow figure. As we consider from the map there is a lateral variation of resistivity value based on this there is highly weathered trachyte and decomposed acidic rock. From the geo-electric section, the resistivity of this layer is seen to vary from70.2 to378.3 Ω-m and its depth extends to 49 m. The resistivity values of the third layer are in the range of 110Ω-m and 10-19 Ω-m. There is a weak zone around the third layer. This relatively higher resistivity response could be due to tuff: yellowish and some part is low resistivity is slightly fractured trachyte, so lower resistivity parts show the groundwater is polluted by the cause of the wastewater transferred through the weak zones drawn on the geoelectrical section to

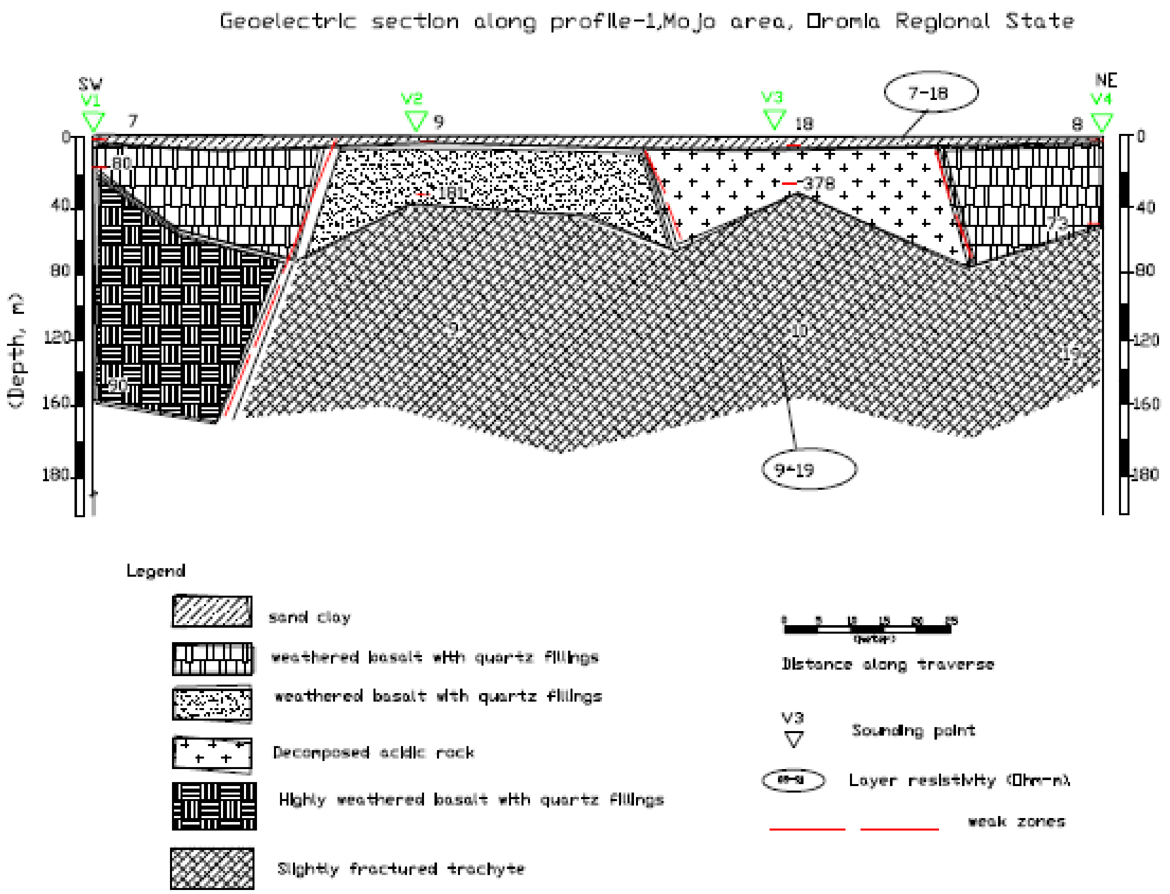

groundwater.

Figure 5-3 Geoelectric section for survey Profile-1.

c) Magnetic Profile Plot

The oscillation of magnetic anomaly profile shows that the symmetrical magnetic stripes across the geological structure (fault, fold, weak zone, etc..), so there are faults can be transferred the wastewater released from the industries around the study area, The other idea is as consider from the anomaly profile there is weak zone or fault between low and high magnetic susceptibility of rock around that area. These weak zones are the cause of wastewater transferred to the groundwater so, groundwater is polluted.

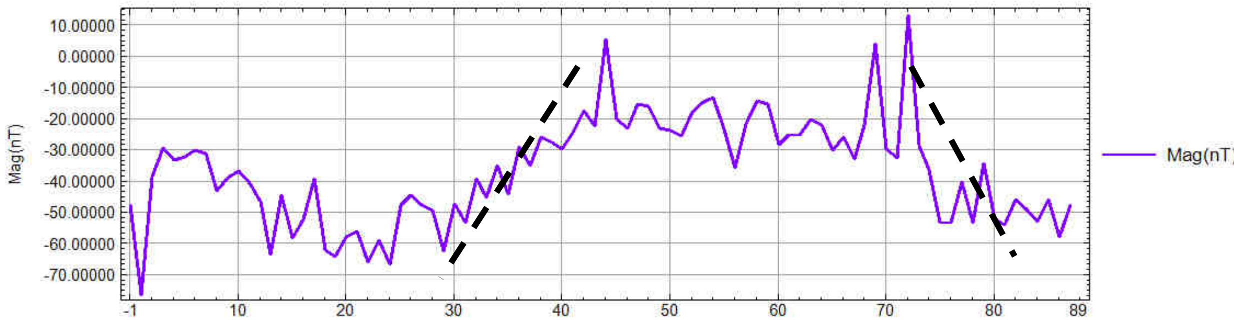

Figure 5-4 Magnetic profile plot for survey Line-1.

Profile-2

a) Apparent resistivity pseudo-depth section

The following pseudo-depth section shows that groundwater is highly polluted based on the value of resistivity. Most parts of this map show low resistivity values less than 10 Ωm and the existence of weak zones along this profile. This weak zone causes for transferring wastewater released from the industries to the groundwater. So groundwater around the study area is polluted.

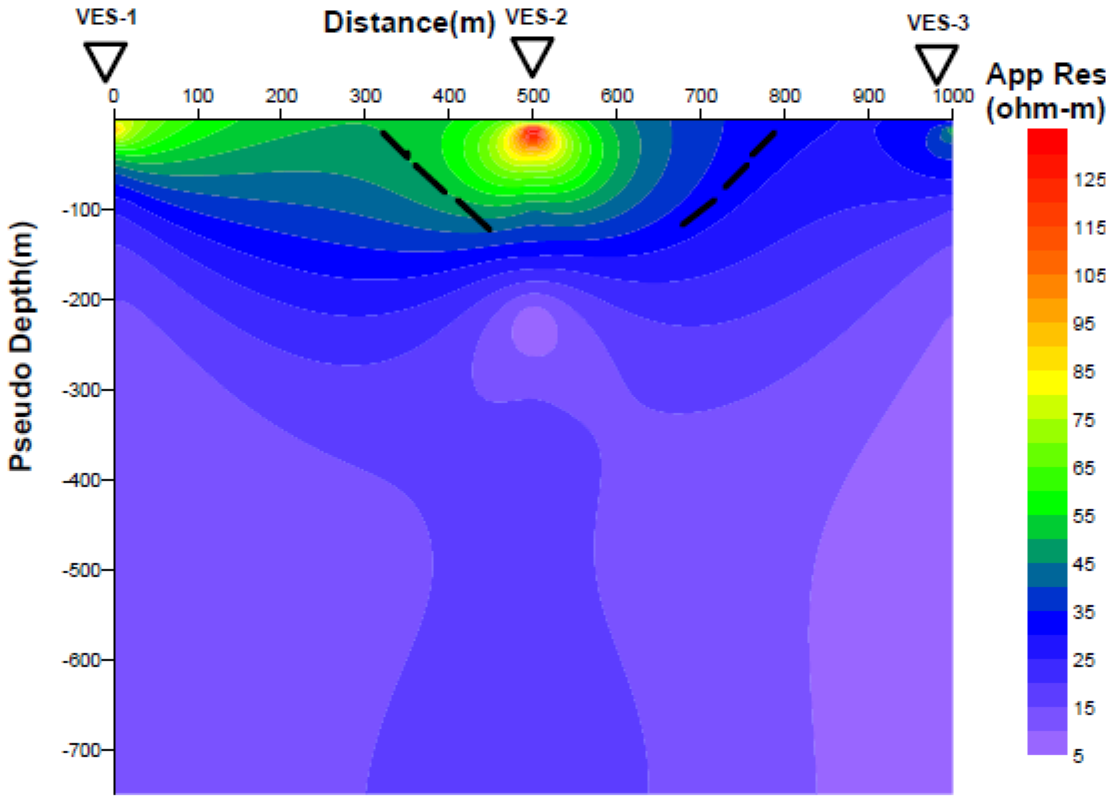

Figure 5-5Apparent resistivity pseudo-depth section for Profile-2.

b) Geoelectric section

The following interpretations are based on the appendix-2 well log data.The first layer is the slightly fractured trachyte that shows relatively low resistivity ranging from 6–16Ω-m and extending to a depth of 3m. The second layer in the geoelectric section exhibits high resistivity values that could be due to tuff: yellowish and this rock also exists in the third layer as we consider from the bellow figure. The resistivity of this layer is seen to vary from100 to189 Ω-m. The third layer is the combination of tuff: yellowish and gravel. From the geo-electric section, the resistivity of this layer is seen to vary from 102.6 and 497. Ω-m and its depth extend to 38m, so there is a weak zone. The resistivity values of the fourth layer are in the range of 20-69 Ω-m. This relatively low resistivity response could be due to highly weathered and fractured trachyte. Based on this lower resistivity value we can identify the pollution of the groundwater.

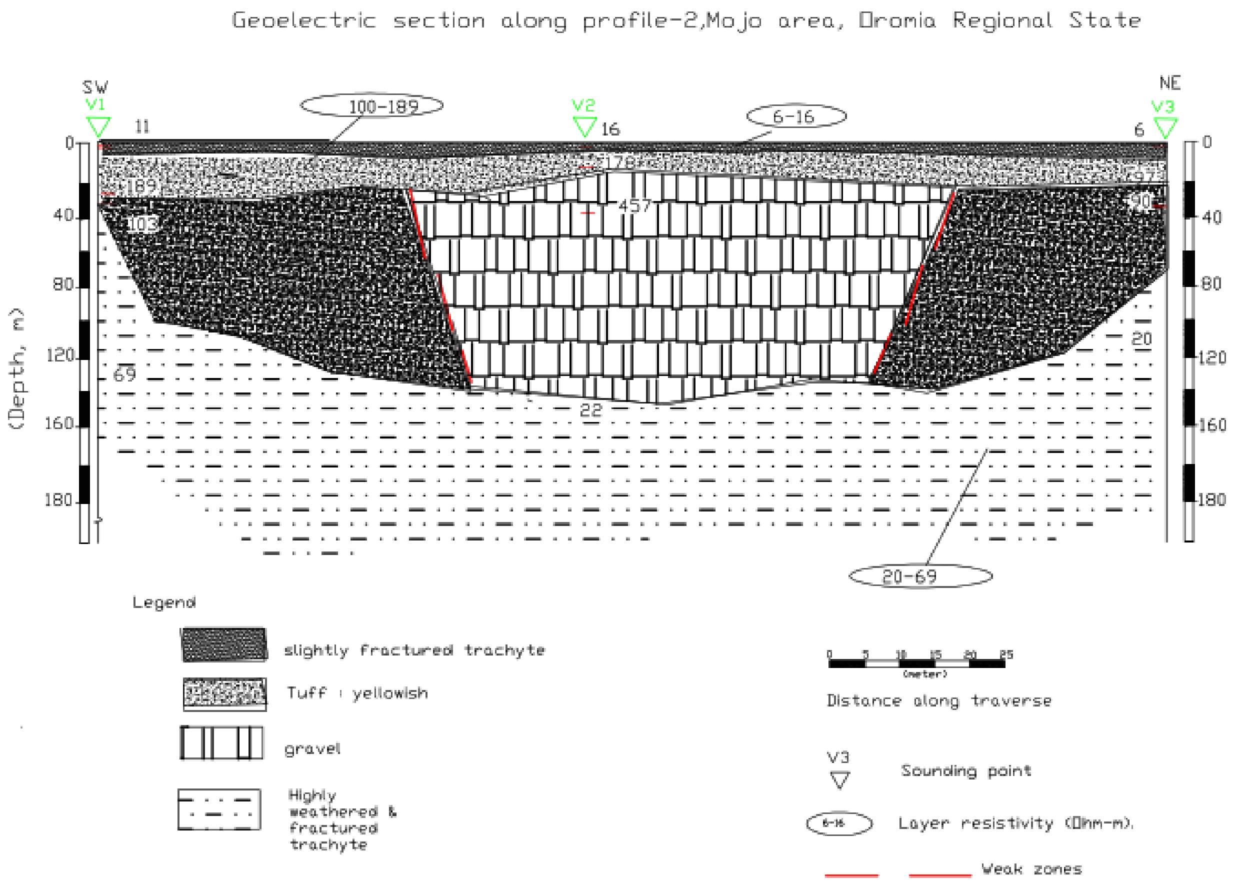

Figure 5-6 Geoelectric section for survey Profile-2.

c) Magnetic Anomaly Plot

As shown in the geoelectrical section (Figure 5-6) the weak zones are starting from the third layer at small depth from the second layer, so the wastewater is easily transferred and pollutes the groundwater. In this magnetic anomaly profile line identified the groundwater has contaminated by the cause of the following weak zones (dash line) on the following anomaly trace identified based on the high and low magnetic susceptiblity.

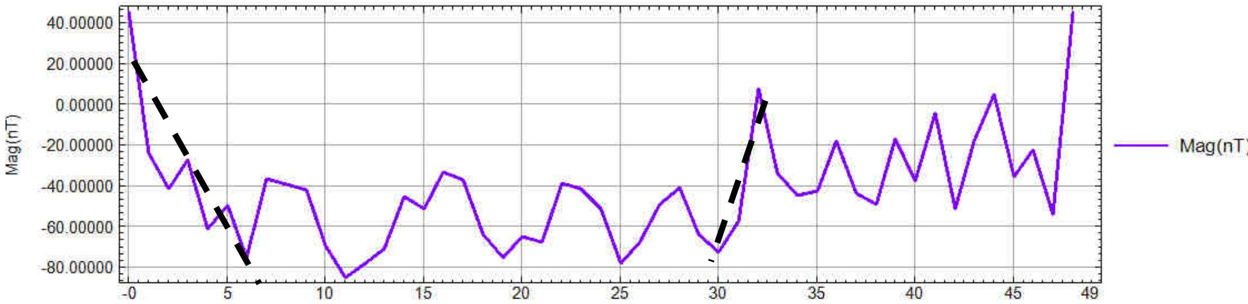

Figure 5-7 Magnetic anomaly profile plot for survey Line-2.

Profile-3

a) Apparent resistivity pseudo-depth section

From this pseudo-depth section the maximum contamination of groundwater identified at deep of the earth based on the resistivity values. The resistivity value of polluted groundwater is less than 10Ωm as the range of rock resistivity values arranged on the resistivity of the color bar in the above section. This map also shows there are weak zones around the study area caused for transferring wastewater released from the industries.

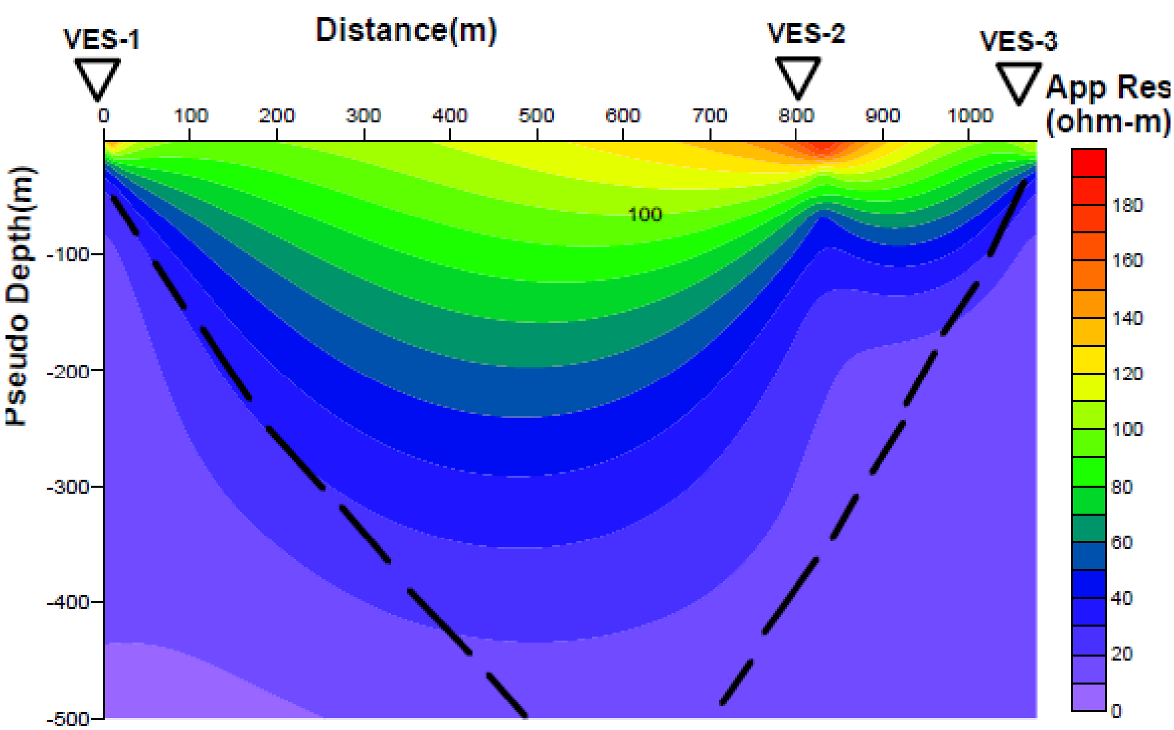

Figure 5-8 Apparent resistivity's pseudo-depth section for survey Profile-3.

b) Geoelectric section and magnetic 2D modeling

The geoelectric section obtained from interpreted VES data that lie on survey Profile-3 is as given in Figure 5-9 (a). The result of the survey hence shows a subsurface consisting of three layers.

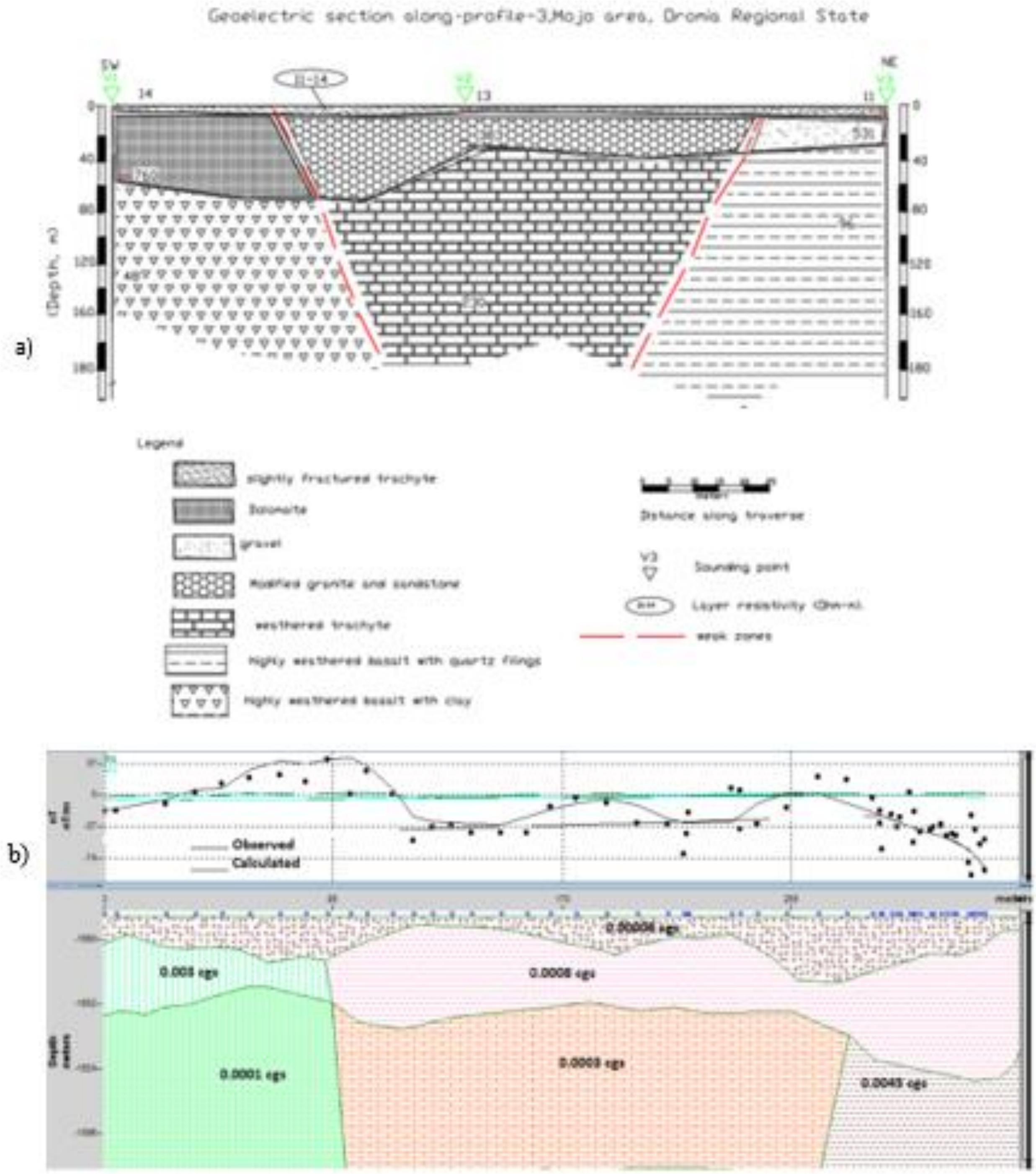

Figure 5-9(a) Geoelectric section and (b) Magnetic 2D model section along Profile-3.

The interpretation of each layers are based on the appendix-2 well log data.The first layer is the slightly fractured trachyte that shows relatively low resistivity ranging from 11–14Ω-m and extending to a depth of 4m. The second layer in the geoelectric section exhibits high resistivity values that could be due to dolomite and gravel. There is a weak zone around the second layer as we consider from the above (Figure 5-9 a). As we consider from the map there is a lateral variation of resistivity value based on this there is a weak zone. From the geo-electric section, the resistivity of this layer is seen to vary from 760 and 531-552 Ω-m and its depth extends to 30 m. The resistivity values of the third layers are in the range of 135Ω-m and 83-95.7 Ω-m. There is a weak zone around the third layer. This relatively higher resistivity response could be due to weathered trachyte, highly weathered basalt with quart filling, and highly weathered basalt with clay. The correlation between the geoelectrical section and the magnetic 2D modeling section for Profile-3 (Figure 5-9 (b)) with error 10% almost both are the same. Both are shows there is a weak zone starting from layer two, so the groundwater is polluted and also identified by the existence of low resistivity.

c) Magnetic anomaly Plot

Most parts of the magnetic anomaly show that the negative values which express the contamination of groundwater around the study area. At 10m there is a fault as consider from the geoelectric section and also there is a weak zone around 10m, and starting from 30m to 40m there is a weak zone, so there is transferred of wastewater released from the industries.

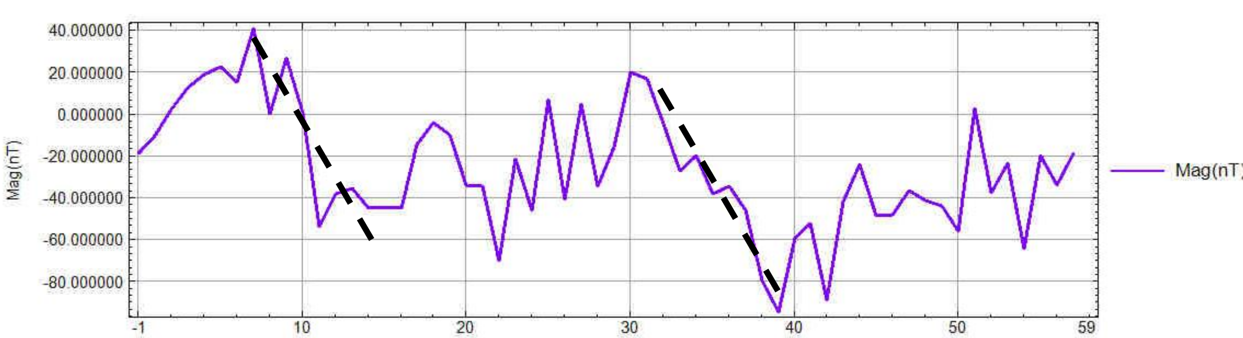

Figure 5-10Magnetic anomaly profile plot for magnetic survey Line-3.

Profile-4

a) Pseudo depth section

The following pseudo depth section shows the weak zone area cause for transferring wastewater released from the industry to the groundwater. As consider the value of rock resistivity the most parts of the map show low resistivity values, so it can identify the groundwater is highly polluted.

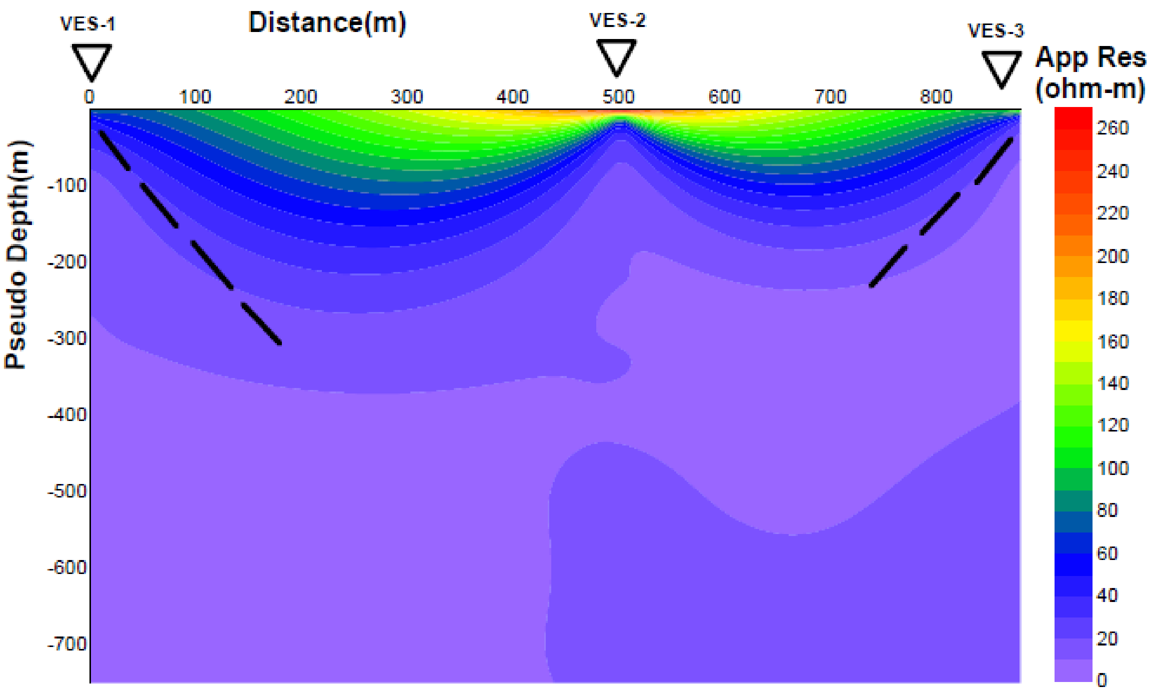

Figure 5-11Apparent resistivity pseudo-depth section constructed from raw data of survey Profile-4.

b) Geoelectric Section

The first layer is the sand-clay that shows relatively low resistivity ranging from 6–11Ω-m and extending to a depth of 6m. The second layer in the geoelectric section exhibits high resistivity values that could be due to pumic light gray and highly weathered and fractured basalt. There is a weak zone around the second layer as we consider from the bellow figure. As we consider from the map there is a lateral variation of resistivity value based on this there is a weak zone. From the geo-electric section, the resistivity of this layer is seen to vary from 64-69 and 146 Ω-m respectively and its depth extends to 20 m. The resistivity values of the third layer are in the range of 115Ω-m and 198.1-208Ω-m. There is a weak zone around the third layer. This relatively higher resistivity response could be due to tuff: yellowish and highly weathered trachyte. All interpretations are based on the appendix-2 well log data. In general, at the top of the layer resistivity value it shows the existence of pollution,but at the bottom layer groundwater is not polluted.

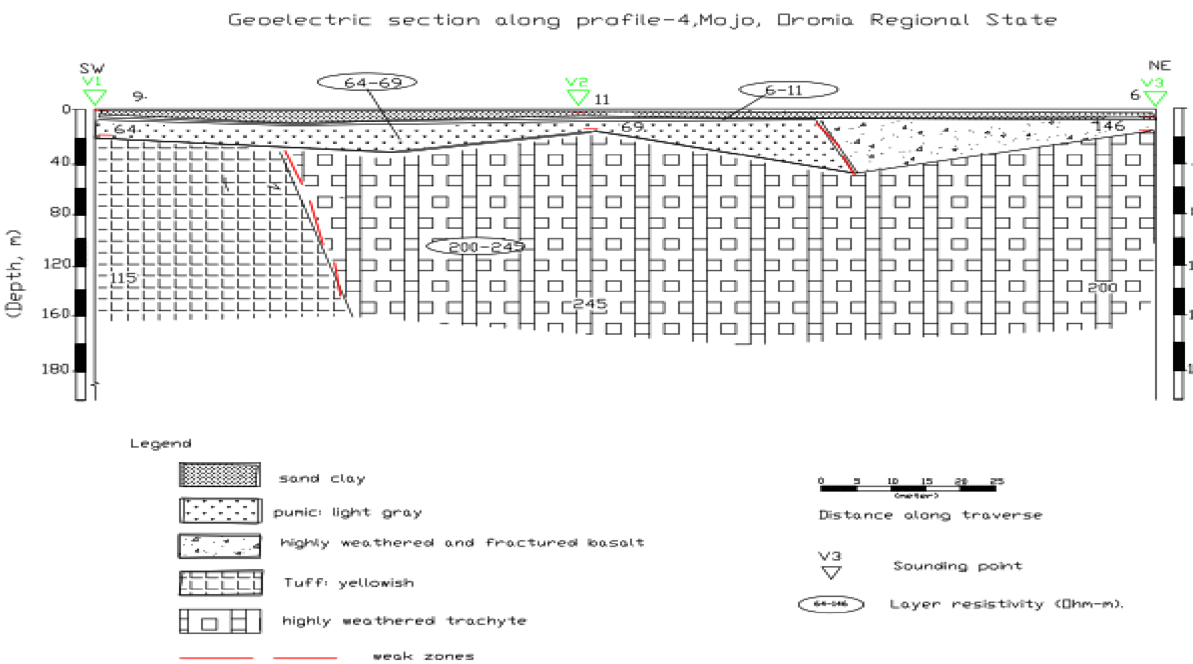

Figure 5-12 Geoelectric section for survey Profile-4.

c) Magnetic Anomaly Plot

The following figure shows groundwater is polluted, because of the maximum magnetic anomaly trace shows negative values or below the zero. In between 25m and 30m, there is a fault. As consider with the above geoelectric section of Figure 5-12 the fault in between VES-2 and VES-3 also around the 20m as follow from the scale bar of the geoelectric section it is the same. The other faults also show on the anomaly trace so wastewater transferred to the groundwater

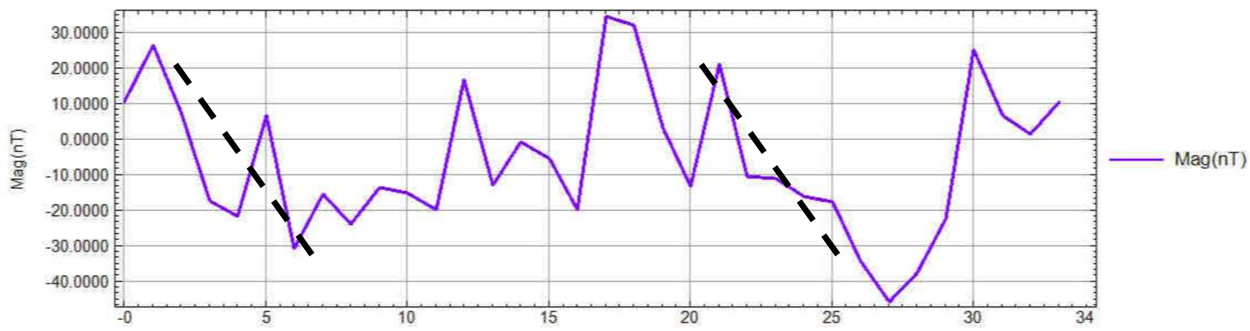

Figure 5-13 Magnetic anomaly profile plot for magnetic survey along Line-4.

Profile-5

a) ***Pseudo-depth section***

The pseudo depth section map for profile -5 shows the existence of weak zones around the study area as the same as the weak zones shown on the geoelectrical section. Those weak zones transfer the wastewater released from the industries into the groundwater, so groundwater is contaminated as consider from the map based on the low resistivity values, because of the resistivity value of polluted groundwater is less than 10Ωm. In general, groundwater is already polluted.

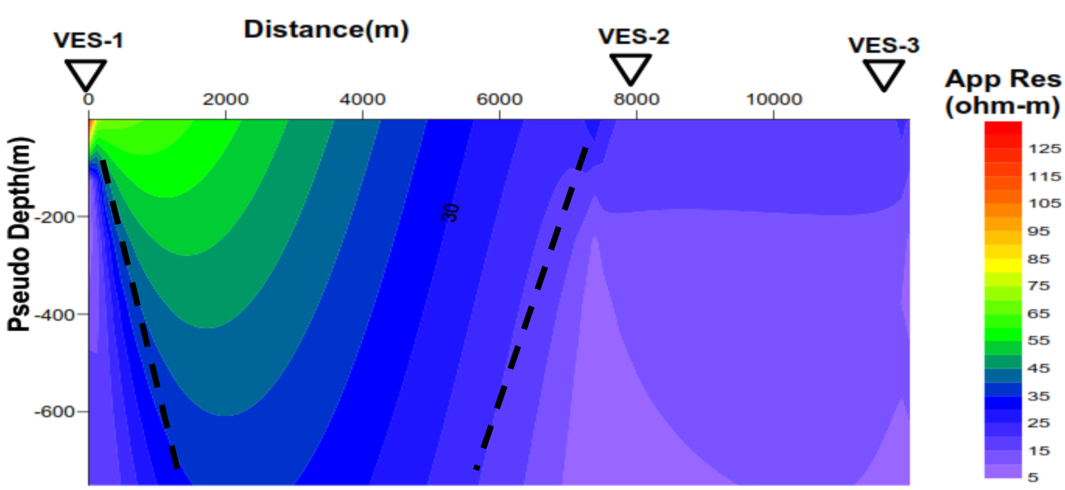

Figure 5-14 Apparent resistivity’s pseudo-depth section for electrical survey Profile-5.

b) Geoelectric section

Figure 5-15 gives the geoelectric section constructed for the VES on survey Line-5. It is seen from the figure that; the first layer is the sand-clay that shows relatively low resistivity ranging from 6–8Ω-m and extending to a depth of 5m. The second layer in the geoelectric section exhibits high resistivity values that could be due to tuff: light gray to yellowish and highly weathered and fractured basalt.

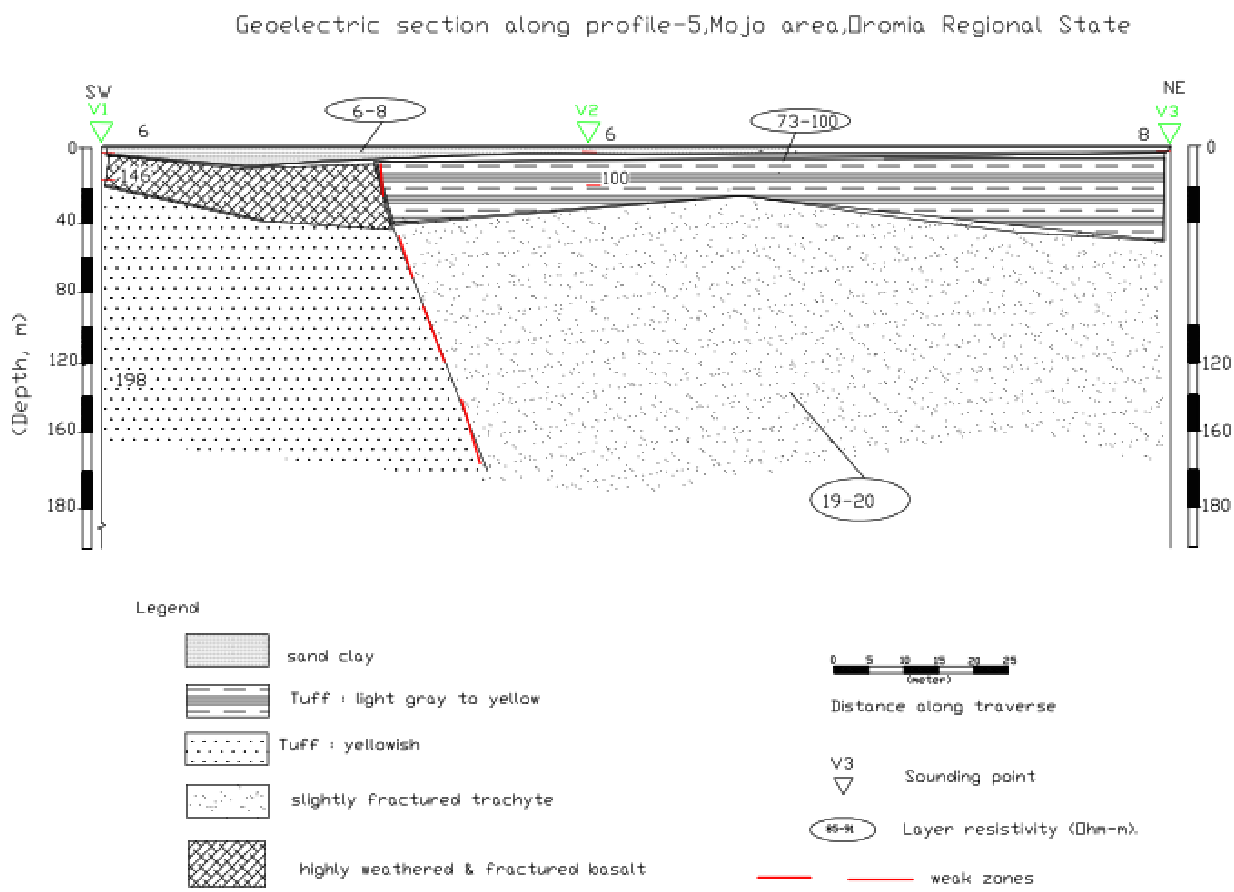

Figure 5-15Geoelectric section for a survey on Profile-5.

There is a weak zone around the second layer as consider from the above figure (5-15) . As we consider from the map there is a lateral variation of resistivity value based on this there is a weak zone. From the geo-electric section, the resistivity of this layer is seen to vary from 73-100 and 146 Ω-m respectively and its depth extends to 48m. The resistivity values of the third layer are in the range of 198.1Ω-m and 19-20Ω-m. There is a weak zone around the third layer. This relatively higher resistivity response could be due to tuff: yellowish and slightly fractured trachyte as borehole data shows the most aquifer is highly weathered and fractured basalt, so the groundwater is polluted because there is weak zone starting from the second layer and also there is low resistivity value at the top of the layer and at the bottom of the layer.

c) Magnetic Anomaly Plot

The pulsed-field magnetization can explain the negative magnetic values in the superconductor starting from 15m, so groundwater contamination is after 15m, because of a contaminant of groundwater is a superconductor and also there is fault starting from the first trace to 15m from magnetic anomaly profile and also the weak zones are shown on the 2D geoelectrical section of above Figure 5-15 also start from the second layer up to 20m as identify from the scale bar of geoelectric section and continuity to the third layer, so wastewater already transferred to groundwater. In general, groundwater is polluted.

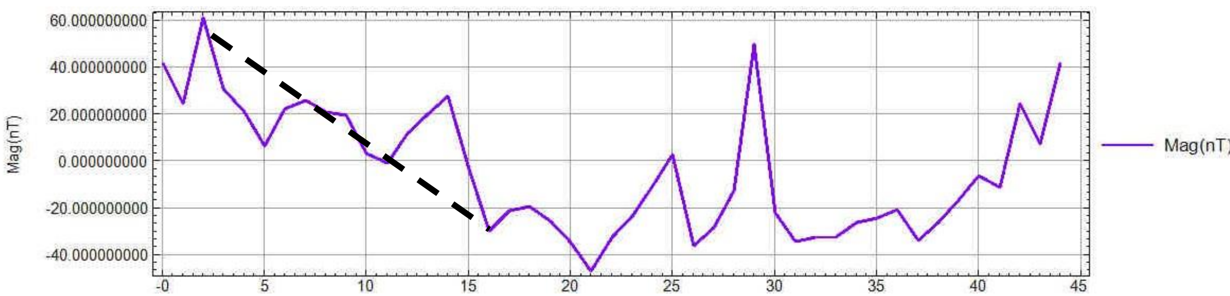

Figure 5-16 Magnetic anomaly profile plot for magnetic survey along Line-5.

Slice and Slice-stacked plots

It is extremely important to view synoptically both the vertical and lateral variation of the electrical resistivity over the area to understand the general and rock-based solid basic structure on which bigger things can be built. This is conveniently gained with effort through the construction of a sliced and then sliced-stacked map from the resistivity values picked up from the vertical electrical sounding data for a few selected (AB/2) values. When the sliced depth sections are arranged in stacked plot form, they provide a simple image that shows the whole picture of the subsurface of the investigated area. The plot resulting in this exercise is given in Figure 5-17. As one can follow from the slice stacking section given in the figure one can identify areas that could be associated with low resistivity potentially water saturated horizons and their extent both laterally and vertically over the surveyed area as well as areas that could be associated with weak zones. From the different slices and the stacking, it is possible to also consider the weak zones as areas for percolation of contaminated water from the River to the different formations, and also, depending on the resistivity values at different depths whether the wastewater released from tannery has indeed penetrated to the groundwater system over the area of study, so the groundwater is already polluted.

Accordingly, for a close examination of these conditions of the ground, i.e. areas of weakness and areas of possible groundwater contamination, the slice-stacked plot of Figure (5-17) is a very convenient way of presenting the data and the depth at which groundwater is polluted. As consider from the value of rock resistivity from the following Figure 5-17 there is groundwater contamination starting from 20m depth .

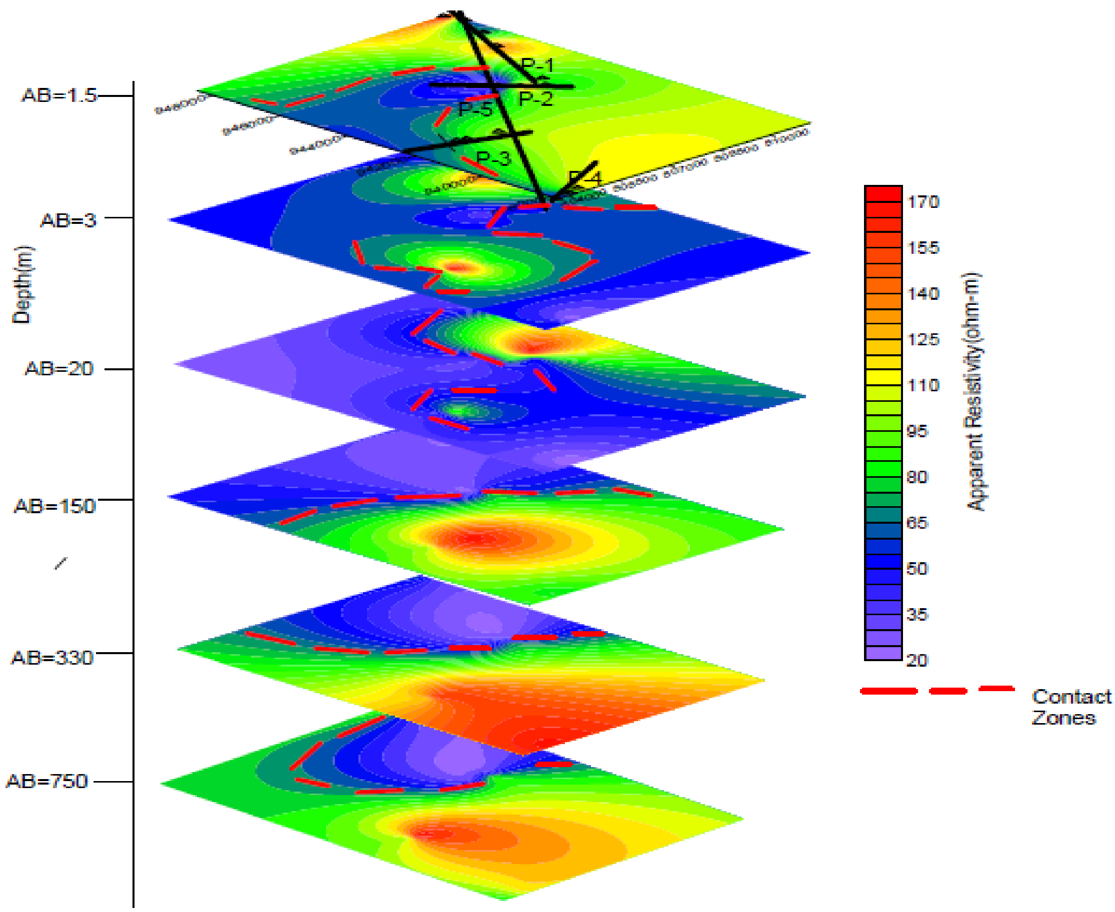

Figure 5-17 Slice-stacked apparent resistivity plot resulting from all VES data of the survey area

CHAPTER SIX

6 CONCLUSIONS AND RECOMMENDATIONS

6.1 Conclusions

The pollution of groundwater identified by using geophysical methods is important to save the life of ecological and public health. The paper identifies the pollution of groundwater by the cause of wastewater released from the tanneries and slaughterhouses transfer through the fault that exists around the study area. The geophysical survey employed in this work has mapped the separation of the subsurface from their electrical and magnetic responses. As certified through a relationship with the lithological log from a nearby borehole, the methods have mapped the different weak zones with a very good resolution. The work shows the viability of, especially, the high resolution vertical electrical sounding to identify the pollution of groundwater and weak zones with very good accuracy, and also the magnetic 2D modeling shows the existence of fault around the study area. As well as the magnetic anomaly profile also shows the area of weak zones causes to transfer wastewater released from the industries to groundwater. The weak zones around the study area can be transferred to the wastewater released from the industries, groundwater can be polluted, so there is spread groundwater contamination around the study area. The other one as considered from the all of the above interpretation starting from pseudo depth section up to slice-stacking as the above structure of all interpretation the most part of the values of electrical resistivity shows less than 10Ωm, so the resistivity value of contaminant of groundwater also less than 10Ωm. Based on this idea the groundwater is highly polluted.

The significance of this research is (a) to investigate the likelihood of pollution of groundwater drinking water around the study area and (b) to express the less treatment of wastewater released from tanneries and slaughterhouses around Mojo town. This means the treatment of wastewater released from the industries is not good, so the groundwater around the Mojo area is a contaminant. In general, the people who exist around the Mojo town are live in very serious conditions. This means when the data collection was done as one seen by our necked eye and by asking information from some people around that area there is a lot of problem regarding wastewater released from the tanneries and slaughterhouses around the Mojo town. The odor of wastewater released from the industries has made it very difficult for the population living around that area and downstream from the areas where the factories are concentrated. The situation is so dire that people downstream have stopped drinking milk because the cows drinking the polluted water produce milk with unpleasant odor and taste and this could be proved to be the case if the milk were tested for its constituents and the chemistry could be attempted to be associated with dominant chemical effluents from the industries. In general, the result of this survey leads to the conclusion that there is a high risk of groundwater pollution around the study area.

6.2 Recommendations

The wastewater released from the industries must be treated before released outside. Based on the values of rock resistivity and weak zones around the study area this paper shows that the groundwater on the Mojo Town- Koka reservoir corridor following Mojo River is highly contaminated. The is a need to prove this fact and quantify the effects through hydrogeological mapping and water chemistry studies of the different water points (boreholes, dug wells, surface water bodies, springs, lakes, etc.) that are found over the whole study area. This could be conducted by taking samples from these points and testing in the laboratory to identifying the physio-chemical characteristics of the waters. It is important to note here that the environmental condition of the study area is very serious and does not give much time to the communities in the area. Local and regional government offices need to take note and plan for remedial measures for the current as well as future pollution of the Mojo River and the water systems downstream of Mojo town.

REFERENCES

Abrha M, Tenalem A and Shifare B. (2015). Impact of Slaughterhouses Effluent on Water Quality of Modjo and Akaki River in Central Ethiopia. *International Journal of Science and Research.***4:**10-15.

Adagunodo,T. A.,Sunmonu,L. A. and Adeniji,A. A. (2015). An overview of magnetic method in mineral exploration. *Journal of Global Ecology and Environment.* **3:**13-28.

Abdullahi, N.K, Osazuwa, I.B and Sule, P.O. (2011). Application of integrated geophysical techniques in the investigation of groundwater contamination: A case study municipal solid waste leachate. *Ozean journal of applied sciences*. **4**:7-25.

Amanial Haile Reda (2016). Physic-chemical characterization of tannery effluent and its impact on the nearby river. *Journal of environmental chemistry and ecotoxicology*. **8**:44-50.

Amanial Haile Reda (2015). Study on the population levels of trace metals from Mojo tannery effluent in the surrounding river water and soil. *Science journal of analytical Chemistry*. **3**:56-60.

Berehanu B. (2007). Impact of Industries and Urbanization on Water Resource in Modjo River Catchment. Unpublished M.Sc. Thesis. Addis Ababa University, Addis Ababa ,Ethiopia.

EIGS (Ethiopian Institute of geological survey) (1984). A report on hydrogeology of the Nazret area. Unpublished report, Addis Ababa, Ethiopia.

EIGS (Ethiopian Institute of geological survey) (1987). A report on hydrogeology of the Northern Main Ethiopian Rift. Unpublished report, Addis Ababa, Ethiopia.

Giday Woldegabriel, James L. A and Robert C. W. (1990). Geology, geochronology, and rift basin development in the central sector of the Main Ethiopia Rift. *Geological Society of America Bulletin.***102:** 439-458.

Gunnarsdóttir, E. L. (2012). *The Earth's Magnetic Field, Research Project*, Physics Department, University of Iceland.

Hunt, C. P.,Moskowitz,B. M. and Banerjee,S. K. (1995). *Magnetic Properties of Rocks and Minerals.* American Geophysical union, America.

Kearey, P., Brooks, M. and Hill, I. (2002). *An Introduction to Geophysical Exploration,* Blackwell Science, USA.

Kebede Amenu (2013). Assessment of water sources and quality for livestock and farmers in the Rift Valley area of Ethiopia: Implications for health and food safety. Unpublished PhD Thesis, University of Hohenheim, Stuttgart, Germany, 120 pp.

Knödel, K., Lange G. and Voigt, H.-J. (2007). *Environmental Geology.* Springer, New York,

Lawal Olubanji A, Adegbite A Ayoade, Oduyiga Olukemi and Adeyanju Adebola (2013). Determination and delineation of groundwater pollution from leachate generated from dumpsite, ijagun community Odogbolu southwestern Nigeria. *American academic and scholarly research journal.* **5**:35-46.

Loke, M.H., Chambers, J.E., Rucker, D.F., Kuras, O. and Wilkinson, P.B. (2013). Recent developments in the direct-current geoelectrical imaging method. *Journal of Applied Geophysics.***95:** 135–156.

Nafyad Serre Kawo and Karuppannan S. (2018). Groundwater quality assessment using water quality index and GIS technique in Modjo River Basin, central Ethiopia. *Journal of African Earth Sciences.***147:** 300–311.

Oyedran Ibrahim, Adewuyi Adeyemi and Gabriel Oladago (2011). Use of geophysical methods in landfill site investigation: A case study of Ibadan, South-Western Nigeria. *New York science journal.***4**:1-10.

Rahman, T., Lebedev M., Zhang Y., Barifcani A. and Iglauer S. (2017). Influence of rock microstructure on its electrical properties: an analysis using x-ray microcomputed tomography. **In:** *Proceedings of the13th International Conference on Greenhouse Gas Control Technologies, GHGT-13,* pp. 5023 – 5031. ELSEVIER, Lausanne, Switzerland

Tenalem Ayenew (2007). Water management problems in the Ethiopian rift: Challenges for development. *Journal of African Earth Sciences.* **48:** 222–236.

Wang Huiwei and Zhang Qianqian (2019). Research advances in identifying sulfate contamination sources of water environment by using stable isotopes. *International journal of environmental research and puplic health*.

Williams M.F. (2016). *Understanding Ethiopia Geology and Scenery*, Springer, Switzerland.

Yazdani, M.Monavari, S.M., Omrani, G.A., Shariate, M. and Hosseini, S.M. (2015). Landfill site suitability assessment by means of geographic information system analysis, pp. 945-956.

Yohannes H, and Elias E (2017). Contamination of rivers and water reservoir in and around Addis Ababa city and actions to combat it. *Environmental pollution and climate change*.**1**:1-12.

Appendix 1. Interpreted VES curves

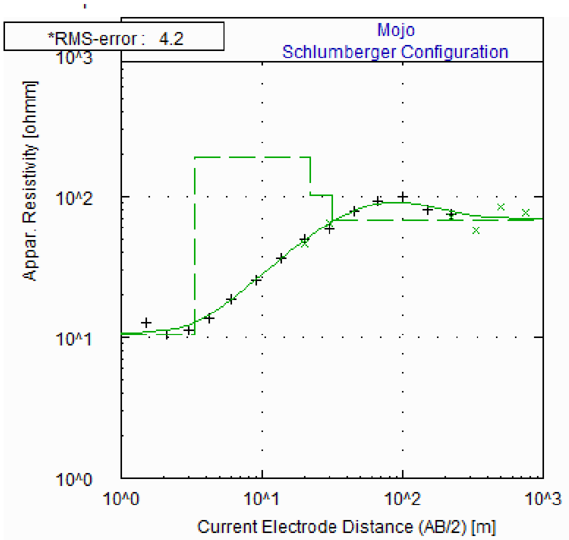

No	Res	Thick	Depth
1	10.6	3.3	3.3
2	189.1	19.0	22.3
3	102.6	9.4	31.7
4	68.7	-.-	-.-

* RMS on smoothed data

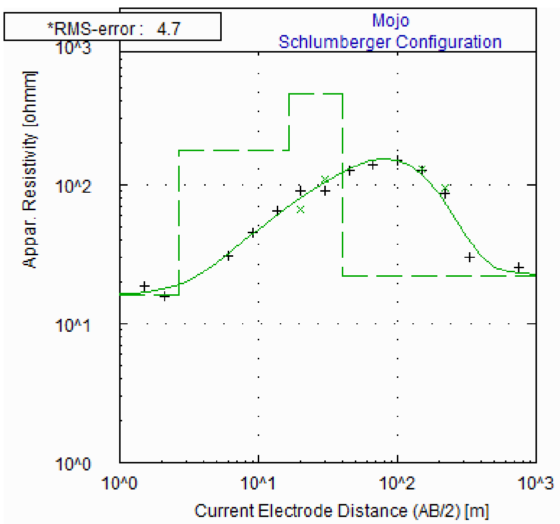

No	Res	Thick	Depth
1	16.3	2.7	2.7
2	178.3	13.7	16.4
3	456.5	24.1	40.4
4	22.0	-.-	-.-

* RMS on smoothed data

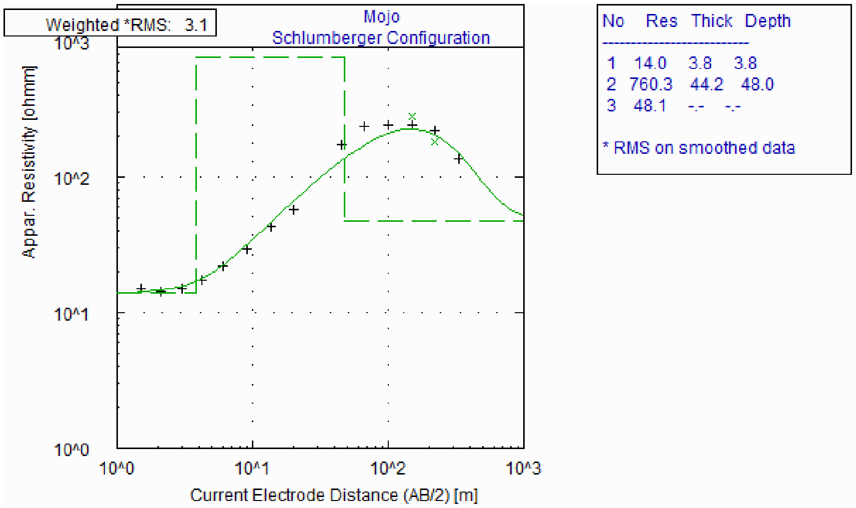
Weighted *RMS: 3.1
Mojo
Schlumberger Configuration
Appar. Resistivity [ohmm]
Current Electrode Distance (AB/2) [m]
No Res Thick Depth
1 14.0 3.8 3.8
2 760.3 44.2 48.0
3 48.1 -.- -.-
* RMS on smoothed data

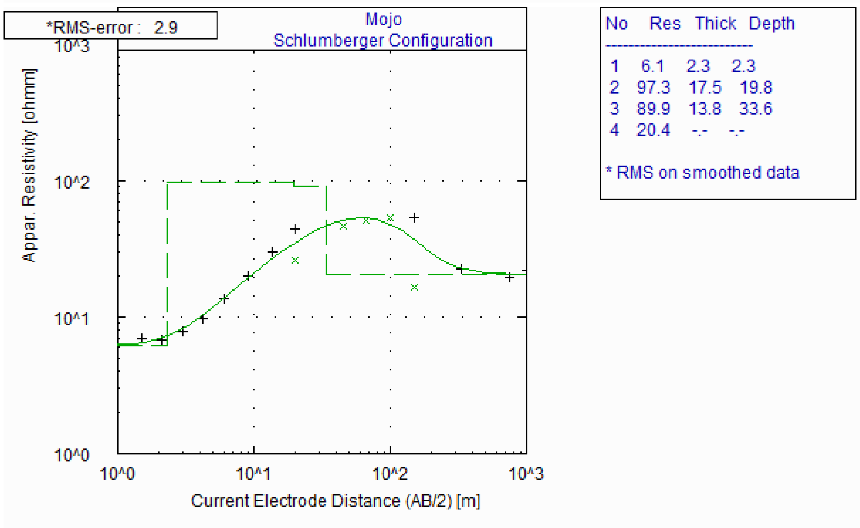
*RMS-error : 2.9
Mojo
Schlumberger Configuration
Appar. Resistivity [ohmm]
Current Electrode Distance (AB/2) [m]
No Res Thick Depth
1 6.1 2.3 2.3
2 97.3 17.5 19.8
3 89.9 13.8 33.6
4 20.4 -.- -.-
* RMS on smoothed data

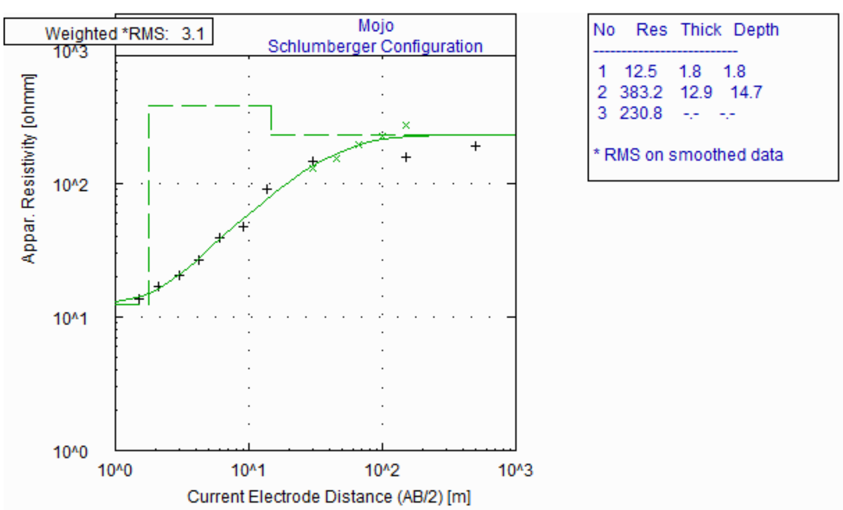
Weighted *RMS: 3.1
Mojo
Schlumberger Configuration
Appar. Resistivity [ohmm]
Current Electrode Distance (AB/2) [m]
No Res Thick Depth
1 12.5 1.8 1.8
2 383.2 12.9 14.7
3 230.8 -.- -.-
* RMS on smoothed data

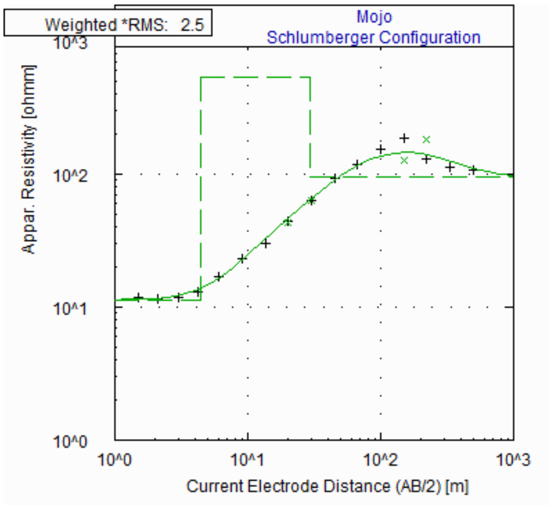

No	Res	Thick	Depth
1	11.4	4.4	4.4
2	531.4	24.8	29.3
3	95.7	-.-	-.-

* RMS on smoothed data

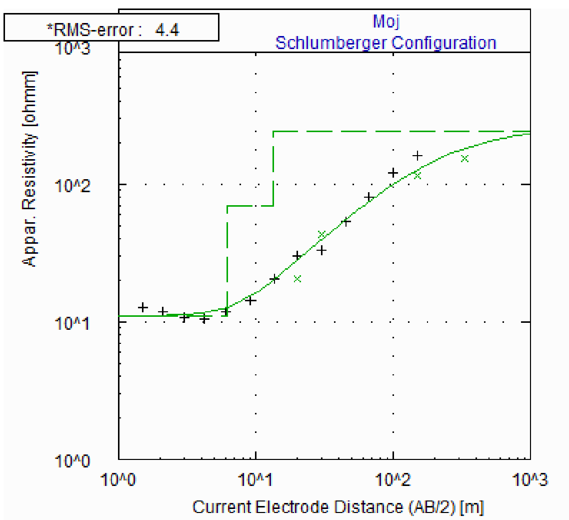

No	Res	Thick	Depth
1	11.0	6.2	6.2
2	69.9	7.0	13.2
3	245.2	-.-	-.-

* RMS on smoothed data

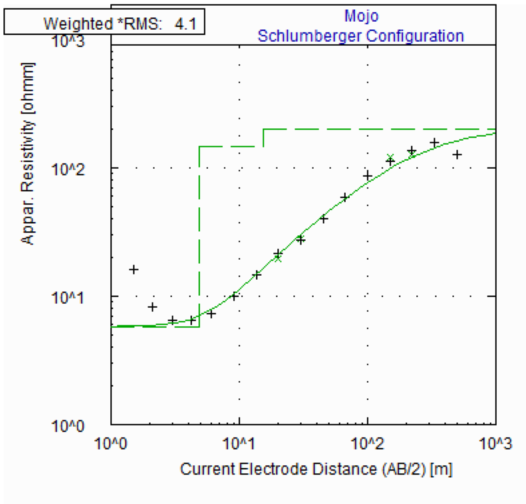

No	Res	Thick	Depth
1	5.8	4.9	4.9
2	145.8	10.4	15.2
3	198.1	-.-	-.-

* RMS on smoothed data

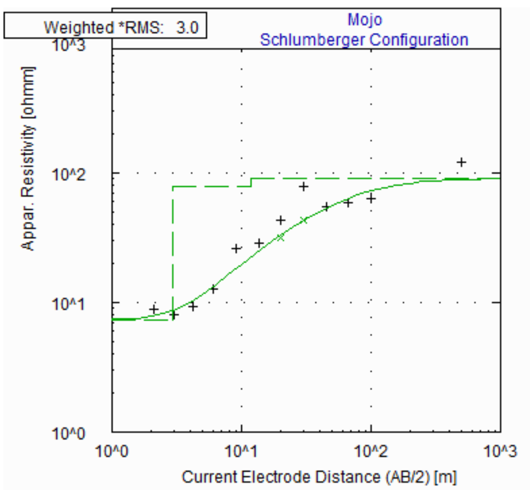

No	Res	Thick	Depth
1	7.3	3.0	3.0
2	79.6	8.9	11.9
3	90.7	-.-	-.-

* RMS on smoothed data

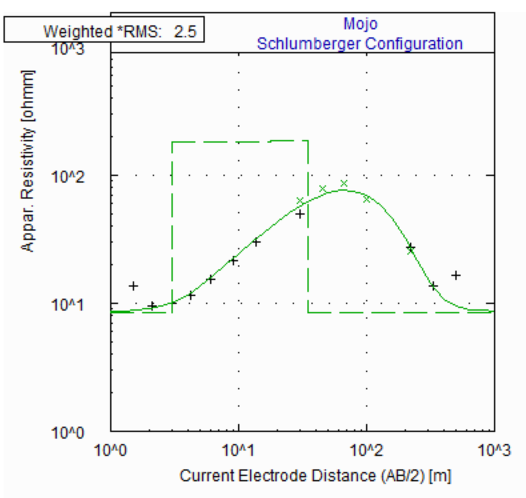

No	Res	Thick	Depth
1	8.5	3.0	3.0
2	180.8	14.7	17.7
3	188.5	16.7	34.4
4	8.5	-.-	-.-

* RMS on smoothed data

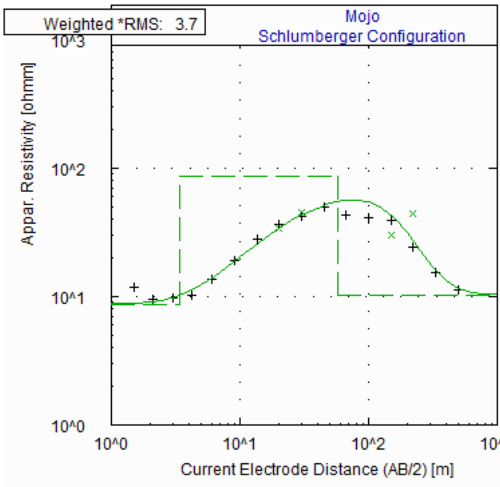

No	Res	Thick	Depth
1	8.7	3.4	3.4
2	87.1	54.5	58.0
3	10.1	-.-	-.-

* RMS on smoothed data

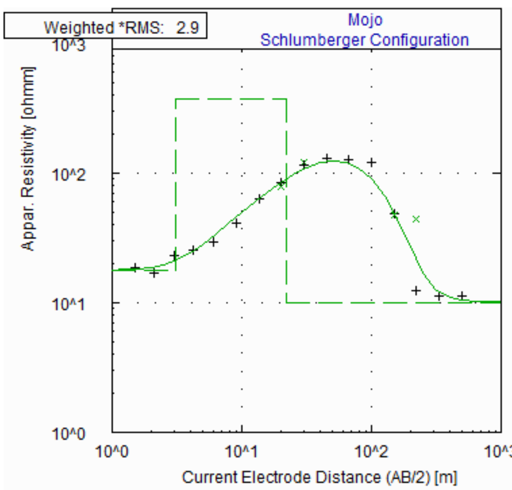

No	Res	Thick	Depth
1	17.7	3.1	3.1
2	378.3	19.0	22.1
3	10.0	-.-	-.-

* RMS on smoothed data

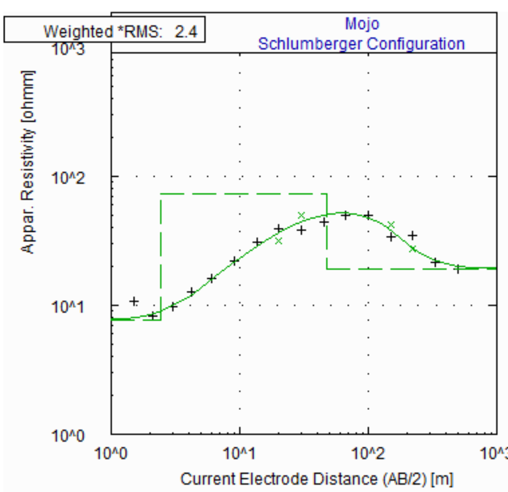

No	Res	Thick	Depth
1	7.7	2.4	2.4
2	73.3	45.4	47.8
3	19.1	-.-	-.-

* RMS on smoothed data

Appendix-2. Well-log Data

Geological Logging

Rock cuttings were collected at each 2m interval and where there were lithological variations are encountered. The cuttings were described properly and water bearing zones were identified.

FROM	TO	LITHOLOGY
0	8	Sandy clay
8	22	Slightly fractured trachyte
22	44	Highly weathered & fractured trachyte
44	54	Highly weathered basalt with clay
54	70	Pumice: light gray
70	78	Weathered basalt with quartz fillings
78	90	Tuff: light gray to yellow
90	96	Highly weathered basalt with quartz fillings
96	142	Tuff: yellowish
142	152	Highly weathered & fractured basalt
152	162	Tuff: weathered
162	188	Weathered basalt with quartz fillings
188	216	Highly weathered trachyte
216	224	Tuff: weathered
224	244	Weathered trachyte
244	292	Weathered basalt with interbeded thin layers of clay
292	302	Highly weathered trachyte
302	322	Moderately fractured basalt with interbeded layers of clay
322	332	Weathered trachyte with clay
332	346	Basalt: weathered
346	358	Decomposed acidic rock